A COMPUTATIONAL STUDY OF DIIODOMETHANE PHOTOISOMERIZATION

Veniamin A. Borin

A Dissertation

Submitted to the Graduate College of Bowling Green
State University in partial fulfillment of
the requirements for the degree of

DOCTOR OF PHILOSOPHY

December 2016

Committee:

Alexander N. Tarnovsky, Advisor

Robert M. McKay
Graduate Faculty Representative

Massimo Olivucci

John R. Cable

ABSTRACT

Alexander N. Tarnovsky, Advisor

This work gives the detailed description of the dynamics and mechanism of the previously unsuspected photochemical reaction path of diiodomethane (CH_2I_2), a paradigmatic haloalkane, which is direct intramolecular isomerization upon the excitation of this molecule to the lowest singlet S_1 state. The previous liquid-phase ultrafast spectroscopy experiments on the UV photochemistry of di- and polyhalomethanes suggest that following excitation of these molecules, the carbon-halogen bond breaks, leading to formation of the initial radical pair. The radical pair, trapped by a solvent cage collapses into an isomer product species with halogen-halogen bond on a picoseconds timescale (1 ps = 10^{-12} s). Yet, the results recently obtained in our research group, clearly suggest that in addition to this conventional, in-cage isomerization process, there is another, unconventional isomerization mechanism, which occurs on a sub-100 fs timescale (1 fs = 10^{-15} s) and does not require the solvent environment around the excited CH_2I_2 solute. Indeed, the ultrafast sub-100 fs timescale observed suggests two main considerations:

- The sub-100 fs photoisomerization in polyhalomethanes is direct, i.e. proceeds via the intramolecular reaction mechanism proceeding without any intermediates (such as a radical pair) and, likely, is mediated by a crossing of excited and ground electronic states.

- The solvent cage may not be needed, because the timescale of the aforementioned isomerization process is shorter than the 100-200 fs timescale for a single collisional encounter between solvent and solute molecules.

Femtosecond transient absorption spectroscopy is a very valuable tool in studying the photochemical reactivity on short timescales. The measured ultrafast time-resolved spectra are complicated by relaxation processes in far from equilibrium solutes, such as intramolecular energy redistribution and flow, and can be understood in detail with the help from state-of-the-art quantum-chemical modeling. Thus, in order to gain the detailed interpretation of the observed (photo)chemical dynamics it is necessary to complement the femtosecond experiments with the modern quantum-chemical computations.

To my mother and friends
Feci quod potui, faciant meliora potentes!

ACKNOWLEDGEMENTS

First, I would like to acknowledge my advisors Dr. Alexander N. Tarnovsky and Dr. Massimo Olivucci for their support and guidance me trough the cobwebs of the Theoretical Chemistry and for the priceless experience they had shared to me. Their great patience allowed me to present this work to you. Also, I am extremely grateful to outstanding scientist and good friend, the former member of Dr. Olivucci research group, Dr. Samer Gozem and Dr. Igor Schapiro, who not only taught me almost everything I know about high-level computations but instilled in me the interest to learn the modern computer techniques as well.

My special acknowledges to my best friends Dr. Mariia Bauman and Dr. Sergey Matveev for their selfless support. They did not let me to stray from the straight path and made me to be concentrated on the issues of the day.

I am thankful to my former and present colleagues in Dr. Tarnovsky research group, namely Darya Budkina, Chris Hicks, Max Panov, Andrey Mereshchenko, Evgeniia Butaeva, Anna Eyzips, Mike Phelan, and Ivan Moreno.

I am very thankful to my committee members, Dr. John Cable and Dr. Robert .

Last but not least, I would like to acknowledge all my classmates and colleges in Center for Photochemical Sciences for their help, support, and valuable discussions throughout these work.

TABLE OF CONTENTS

LIST OF TABLES

LIST OF FIGURES

LIST OF SCHEMES

CHAPTER 1: THEORETICAL BACKGROUND

Molecular dynamics

Molecular dynamics (MD) is one of the dominant methods of computer simulation of physical processes. Complemented by the electronic structure methods, the MD method is the primary research tool for systems with a significant number of the degrees of freedom.[1-3] The MD method allows to simulate the detailed microscopic picture of the internal mobility of macromolecules. The method is based on the calculation of classical (Newtonian) equations of motion in the space of coordinates and momenta of atoms. Within the method, a molecule under study is described as a system of interacting classical particles. The most widely used algorithm for numerical integration of the classical equations of motion is the so-called velocity Verlet algorithm.[4,5] Let's consider the motions of atoms described through the velocity Verlet algorithm as implemented in MOLCAS program package.[6] Let $r_i(t), \vec{v_i}(t),$ and $\vec{a_i}(t)$ be, respectively, the coordinate, the velocity, and the acceleration of the i-th particle at a time t. Now, setting the initial values of coordinates, velocities, and defining a time step (Δt) one can run a classical molecular dynamics simulation of a molecular system as it shown below.

1. The initial step is evaluation of the $\vec{a_i}$ value according to the Newton's Second law:

$$\vec{F_i}(t) = m_i \vec{a_i}(t) \Rightarrow \vec{a_i}(t) = \frac{\vec{F_i}(t)}{m_i} \qquad\qquad 1$$

The force $\vec{F_i}$ is nothing but the nuclear gradient of the potential energy surface (PES):

$$\vec{F_i} = -\nabla_i U = -\frac{d\langle \Psi | \hat{U} | \Psi \rangle}{dr_i} \qquad\qquad 2$$

where Ψ is a wavefunction of the system. The force can be computed either analytically or numerically by an appropriate method of computational chemistry.

2. The next step is to calculate the new set of coordinates:

$$\vec{r_i}(t + \Delta t) = \vec{r_i}(t) + \vec{v_i}(t)\Delta t + \frac{\overline{a_i}(t)}{2}\Delta t^2 \qquad\qquad 3$$

3. For new set of atomic coordinates the accelerations $\vec{a_i}(t + \Delta t)$ are computed according to equations I.1 and I.2.

4. Finally, the atomic velocities for new geometry can be computed:

$$\vec{v_i}(t + \Delta t) = \vec{v_i}(t) + \frac{\overline{a_i}(t) + \overline{a_i}(t + \Delta t)}{2}\Delta t \qquad\qquad 4$$

The steps 1 – 4 are being repeated as many times as needed.

To be simple, the classical molecular dynamics represents the "classical" evolution of the system on the molecular PES, which is computed by a quantum-chemical method of choice, but no interaction between different PESs are taken into account. Due to the fact that the majority of photochemical processes are non-adiabatic, i.e. involve electronic transitions between different PESs, instead of classical molecular dynamics it makes sense to utilize the semiclassical MD simulation. The term "semiclassical" means that the atomic motion on a PES is described "classically" by means of the velocity Verlet algorithm, but the transitions between different PESs (surface hops) may occur. The most common method to take these hops into account is the Tully surface hopping (TSH) technique.[7-10] The TSH theory is quite simple: it is a matter of the knowledge of the time-dependent Schroedinger equation:

$$-i\hbar \frac{d\Psi(r,q,t)}{dt} = \hat{H}\Psi(r, q, t) \qquad\qquad 5$$

where $\Psi(r, q, t)$ is a total wavefunction of the system under consideration, and r, q, and t are the nuclear coordinate, electronic coordinate, and time, respectively. According to the Completeness theorem (*a set of the eigenfunctions of Hermitian operator is complete, i.e. any other function, satisfying the same boundary condition and defined in the same interval can be expressed via a linear combination of the eigenfunctions of this Hermitian operator*), this wavefunction can be

represented as a linear combination of the eigenvectors of the Hamiltonian operator of the system:

$$\Psi(r, q, t) = \sum_i c_i(t)\phi(r, q) \tag{6}$$

The functions $\varphi(r,q)$ correspond to the different electronic states. Substitution of equation 6 into 5 yields:

$$i\hbar\frac{dc_j}{dt} = \sum_i c_i(H_{ij} - i\hbar h_{ij}\frac{dr}{dt}) \tag{7}$$

where h_{ij} is the non-adiabatic coupling vector:

$$h_{ij} = \langle\phi_i|\nabla_r\phi_j\rangle \tag{8}$$

The surface hop may occur at any time and depends on how the probability $|c_j|^2$ changes. The magnitude of this change is:

$$\frac{d|c_j|^2}{dt} = \sum_i [\frac{2}{\hbar}Im(c_i c_j^* H_{ji}) - Re(c_i c_j^* h_{ji}\frac{dr}{dt})] \tag{9}$$

Transferring dt to the right part of the equation 9, for small interval of time, we obtain the explicit equation of the hop probability:

$$P_{j\rightarrow i} = \frac{1}{|c_j|^2}[\frac{2}{\hbar}Im(c_i c_j^* H_{ji}) - 2Re(c_i c_j^* h_{ji}\frac{dr}{dt})]dt \tag{10}$$

It must be noted that the summation is over all $i \neq j$ Thus, one need n potential energy surfaces to evaluate $n-1$ hopping probabilities (from the given state to another ones). Next, the program compares each probability with a random number and. If the evaluated probability is bigger than this random number, the surface hopping event is considered to have taken place. The amazing elegance of this technique is that it is in line with the uncertain and probabilistic nature of quantum mechanics. In fact, even if the probability of a certain process is known, say 90%, still no one can predict the result of a single measurement! One can only be said is that in a statistically significant number of experiments, 90% outcomes would show that this process has occurred and 10% outcomes would show that it has not.

This poses a new challenge and new opportunities. A single MD simulation of a chemical reaction does not make too much sense because it represents only one of a number of many ways the reaction may proceed. Instead of running a single MD simulation one needs to generate an ensemble of N initial conditions (nuclear coordinates $\mathbf{r_i}$ and velocities $\mathbf{v_i}$) and run the N number of the independent processes. The result of such simulation can be, for example, a reaction product yield (or, a quantum yields in case of a photochemical process), defined as a ratio of trajectories, which gave a certain product, to the total number of trajectories. Also, the difference in initial conditions may affect the lifetimes of products and intermediates, so it is important to analyze the whole ensemble of trajectories.

The popular method of generating the initial conditions is thermal sampling. The given temperature is converted to the vibrational (kinetic) energy and then randomly distributed over normal modes of the molecule of interest. Afterwards, the program distorts the molecular geometry in accordance with the degree of vibrational excitation and computes the nuclear gradients. Finally, according to equation I.1, I.2, and I.4, the gradients are recomputed to obtain the nuclear velocities.

Multiconfigurational and multireference quantum chemistry

One of the most important effects in computational chemistry is the electron correlation. Electron correlation is the interaction between electrons in the electronic structure of a quantum system, and is critical for the accurate and quantitative evaluations of molecular energies. There are two types of electron correlation effects: dynamical and static correlations. Dynamical correlation is a correlation of the movement of electrons due to instantaneous same-charge (Coulomb correlation) and same-spin (Fermi correlation) repulsion. The static correlation becomes important in the neighborhood near-degenerate or intersection potential energy surfaces,

where the wavefunction of the system cannot be described by a single Slater determinant.

The simplest way to account for electron correlation is to use a configuration interaction (CI) methodology.[11-13] In this case, the wavefunction is expressed as a linear combination of Slater determinants (or configurations):

$$\Psi_{CI} = C_0\Phi_0 + \sum_N C_N\Phi_N + \sum_N \sum_M C_{NM} \Phi_{NM} + \cdots \qquad 11$$

where Φ_N are the Slater determinants, obtained from the reference (Φ_0) by promotion of an electron from one orbital to another, the third term in 11 stands for promotion of two electrons e.t.c. The set of C_K is solved variationally.

The simplest variant of CI is so-called configuration interaction singles (CIS). It is obtained by contraction of equation 11 to the first two terms only. The CIS is computationally inexpensive, and as a result, can be applied to excited state simulations. The CIS treats the static electron correlation, but no improvement of the ground state energy can be made. This is a consequence of the Brillouin theorem, which states that the Hamiltonian matrix element between the ground state and any of singly excited determinants is zero:

$$\langle \Psi_0 | \hat{H} | \Psi_i \rangle = 0 \qquad 12$$

So, no dynamic correlation will be recovered. To overcome this problem one can contract equation 11 to include the third term, which yields the configuration interaction singles and doubles (CISD). This method treats two-body (due to pairwise electron-electron interaction) effects, but also is more computationally demanding. If all possible excitation are taken into account we will obtain the full configuration interaction (FCI) treatment.

The FCI method provides the numerically exact solution (within the given basis set) of Schroedinger equation under the non-relativistic time-independent approximation. It must be mentioned that this method is applicable to very small systems, containing a tractable number of

electrons and orbitals, for example, in case of CH_2I_2 with 6-311G** basis set (114 electrons and 165 orbitals) one needs to optimize the series of $2.68 \cdot 10^{88}$ Slater determinants, which is impossible even with using current supercomputers.

To simplify the computations it makes sense to determine the so-called active configuration space, i.e. a set of high-lying occupied and low-lying vacant orbitals involved in the electronic transitions. If within this space all possible n-tuple excitations are allowed, it is called a complete active space self-consistent field (CASSCF).[14] The rest of the orbitals do not participate in the electronic transitions. The CASSCF method, as well as Hartree-Fock method, poorly describes dynamic electron correlation, but the multiconfigurational nature of the wave function is well suited for accounting static correlation, and, therefore, CASSCF works well in the regions where different electronic states are degenerate.

Despite the fact that CASSCF does not give dynamic electron correlation, this method provides a good starting point for further improvements. The much more accurate, but also much more time-consuming, is the multireference (MR) approach, which contracts the CASSCF wavefunction. There are a lot of possible ways to improve the reference function to take into account dynamic correlation. The multireference configuration interaction (MRCI) performs the excitations (usually, single and double only) on top of the CASSCF wavefunction. As a result, the MRCI method gives a more balanced description of the correlation on the ground and excited states, but the computational cost increases as well.

Another approach is called multireference perturbation theory (MRPT). As well as in the case of MRCI, the CASSCF wavefunction is used as a reference function, which is followed by computation of the energy correction in accordance with perturbation theory. In principle, one can use a correction of any order (MR-MP3, MR-MP4[16-19]), but since the perturbation series is

rapidly converges, the common case is to confine it to include the second order only – MRPT2. This technique has a number of flavors (CASPT2,[20] (X)MCQDPT2,[21] NEVPT2[22-24]). The CASPT2, as it is implemented in MOLCAS program package, is one of the most popular types of MRPT and is thought to be 'a gold standard' of modern computational photochemistry.[25]

CASPT2 is the equivalent of the MRCI method in a sense that both of them provide the correction to the zero-order wavefunction. But if MRCI performs "physical" excitations (when each configuration is created and stored in the computer memory by a quantum-chemical program), CASPT2 evaluates the electron-electron and state-state interactions "virtually", and therefore, it is much less time-consuming and computationally demanding.

It must be mentioned that all MRPT methods have a problems in the regions of near-degeneracy. It can be clearly seen from the expression of the second order energy correction:

$$E_I^{(2)} = \sum_J \frac{\langle I|\hat{V}|J\rangle\langle J|\hat{V}|I\rangle}{E_I^{(0)}-E_J^{(0)}} \qquad\qquad 13$$

where I and J are the different electronic states, E_I and E_J are the corresponding energy, and $\hat{V}$ is a perturbation operator. If energies E_I and E_J are close to each other, the denominator tends to be zero, and as a result, the energy correction non-physically increases. This effect is known as intruder states (IS). To overcome the IS problem one can use the imaginary denominator shift – the small constant δ, which, when added to the denominator of 13, resolve the issue of the IS.

As any other methods, MRPT has a number of disadvantages and limitations:

1. The MRPT method will give the accurate energies of the ground and excited states if and only if the reference CASSCF wavefunction is correct. In the cases, when the CASSCF method is inapplicable to the system of interest, MRPT becomes inapplicable as well.

2. None of the MRPT methods are variational, i.e. the exact energy is not necessarily the lower limit of the calculated energy.

3.   None of the MRPT methods are "black-box", i.e the user must clearly understand the features of a system before run MRPT.

4.   Due to the complexity of the expression for energy, the analytical nuclear gradients are unavailable. One needs to perform $6N$ (N is a number of atoms) single-point energy evaluations to compute the numerical gradients via finite-difference. It must be mentioned, that Shiozaki *et al.*[26] after almost 2.5 years of work produced an analytical gradients for MOLCAS' type CASPT2, and this technique will be hopefully available soon.

Accounting for solvation effects

The accuracy of quantum chemical methods in predicting the chemical reactivity in the liquid phase can be significantly improved by including the solvation effects in the simulations. All solvation models can be divided by two families: implicit and explicit solvation.

The implicit solvation model considers solvent as a dielectric continuum in which the molecule of an interest is placed in the cavity of solvent. This model does not require time-consuming calculations that determines its wide usage. However, there is a great diversity of the implicit solvation descriptions depending on the definition of a solvent shell volume and the description of solute-solvent interactions. The most common among them are the polarized continuum model (PCM)[27,28] and its modification, the conductor-like polarizable continuum model.[29,30]

All continuum-based solvation methods can be thought as a type of perturbation theory. The Schroedinger equation can be written as:

$$(\hat{H}_0 + \hat{V}(M,S))\Psi = E\Psi \qquad\qquad 14$$

where $\hat{H}_0$ is a zero-order Hamiltonian operator of the molecule of interest and $\hat{V}(M,S)$ is an operator that describes the interaction between a solute M and a field created by the solvent

molecules S.

To find free energy G one needs to minimize the variational functional:

$$G = \frac{\langle \phi | \hat{H}_0 + \hat{V}(\rho) | \phi \rangle}{\langle \phi | \phi \rangle} \qquad\qquad 15$$

The functional $\hat{V}(\rho)$ is a potential, which depends on the charge distribution $\boldsymbol{\rho}$, and $\boldsymbol{\phi}$ is a trial function. The electrostatic problem of a charge distribution in a cavity surrounded by a continuum dielectric can be solved by Poisson equation:

$$4\pi\rho(r) = -\nabla \cdot [\epsilon(r)\nabla\phi(r)] \qquad\qquad 16$$

The solvation energy in the polarizable continuum model is found a sum of the following three terms:

$$G_{solv} = G_{es} + G_{dr} + G_{cav} \qquad\qquad 17$$

These components represent the electrostatic (G_{es}) and the dispersion-repulsion (G_{dr}) contributions to the free energy, and the cavitation energy (G_{cav}), which is the energy required to create the cavity in the dielectric continuum. All three terms are calculated using a cavity defined through interlocking van der Waals (vdW) spheres centered at atomic positions. The reaction field is represented through the point charges located on the surface of the molecular cavity. In this model, the vdW-surface is constructed from spheres located on heavy (all elements, except for hydrogen and helium) elements only. The vdW-radius of each atom is a function of the atom type, the atom connectivity, the overall charge of the molecule, and the number of attached hydrogen atoms.

The continuum models have three main disadvantages:

1.   In the systems, where non-electrostatic (such as van der Waals interactions) effects dominate the solute-solvent interactions, none of the continuum models will work properly.[31,32]

2.   If specific solvent-solute interaction, such as hydrogen-bonding, or charge transfer are

present, continuum models will ends up with incorrect results.

3.   The main assumption one needs to make when using implicit solvation models is that the field created by solvent molecules is continuous, which is not true on a molecular scale.
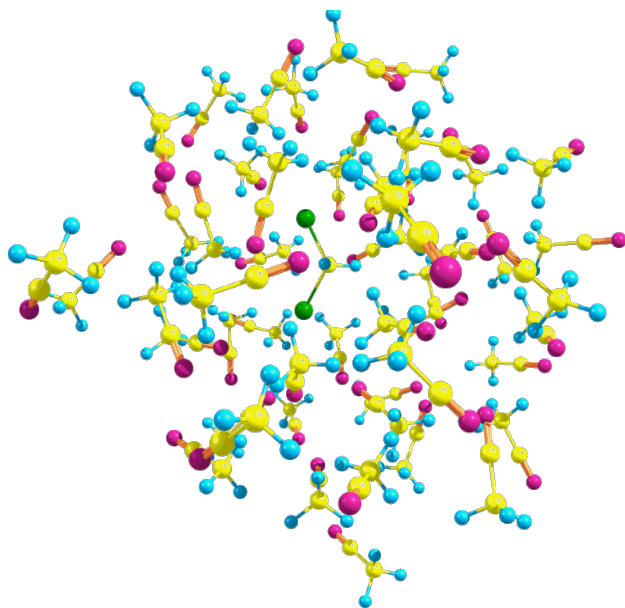
Figure 1.1. An example of a CH_2I_2 molecule in a solvent cage of acetonitrile.

In contrast to the continuum models, the explicit model is based on using a large number of discrete solvent molecules, see Figure 1.1. This technique is widely used for carrying out simulations in the condensed phase, especially in biological environments. Moreover, this model is capable of describing specific solute-solvent interactions, e.g. H-bonding. The calculations using the explicit solvation model converge slowly because of the large number of particles involved. Because there is impossible to provide the same level of quantum chemical description to the solute and all solvent molecules involved, the *ab initio* description is provided for solute only, but the solvent is treated by the molecular mechanics force-field. This hybrid method is called QM/MM (Quantum Mechanics/Molecular Mechanics). The QM/MM approach was introduced in the 1976 paper of Warshel and Levitt.[33] They won Nobel Prise in Chemistry in

2013 for "the development of multiscale models for complex chemical systems". The QM/MM method combines together the accuracy of quantum mechanics and the efficiency and speed of molecular mechanics.[34-37] As it was mentioned above, the whole system is divided into two parts: the solute and the solvent, which are described by quantum mechanics and molecular mechanics respectively. The energy of a QM/MM system can be defined as follows:

$$E = \langle \Psi | \hat{H}_{QM} + \hat{H}_{MM} + \hat{H}_{QM/MM} | \Psi \rangle \qquad\qquad 18$$

where $\hat{H}_{QM}$ is a regular Hamiltonian operator of an isolated QM subsystem; $\hat{H}_{MM}$ is the energy of an isolated MM subsystem defined by the corresponding force-field; $\hat{H}_{QM/MM}$ stands for the interaction between QM and MM subsystems. This term can be explicitly as:

$$\hat{H}_{QM/MM} = E_{VDW} + \sum_i q_i \int \frac{\rho(r)}{r} dr \qquad\qquad 19$$

where E_{VDW} is a van der Waals interaction energy, and the second term expresses the electrostatic interaction between the continuous charge distribution of the QM- and the discrete charge distribution of the MM- sub-systems.

We must remember two important assumptions:

1.   The energy of the MM part does not depend on the charge distribution in the QM part.

2.   No chemical changes may occur in MM part.

Despite these weaknesses, the QM/MM technique provides a valuable tool for studying the molecular dynamics in a liquid phase or in protein environment. It is a matter of fact that molecules in condensed media can undergo the intermolecular vibrational relaxation, i.e. the excess of the vibrational energy can be transferred from the molecule to the environment. This transfer stabilizes the forming reaction product. In contrast to the continuum solvation models, QM/MM yields a "physical" description of atoms, which is necessary for the kinetic energy transfer.

Conical intersections

One of the most important approximations in quantum mechanics is that by Born and Oppenheimer (BO approximation). This approximation, which is also known as abiabatic, is based on the fact that the electrons move significantly faster than nuclei, and therefore, one can consider the total wavefunction of a system as a product of nuclear and electronic parts:

$$|\Psi_{tot}(R,r)\rangle = |\Psi_{nuc}(R)\rangle|\Psi_{el}(R,r)\rangle \qquad\qquad 20$$

Here, the electronic part is a function of the electronic coordinates (r), but also depends on the nuclear positions (R) as parameters. In other words, the electronic wavefunction is found for every fixed molecular geometry. Within the Born-Oppenheimer approximation, the Hamiltonian operator can be expressed as:

$$\hat{H} = -\sum_n \frac{1}{2M_n}\nabla_n^2 - \sum_i \frac{1}{2}\nabla_i^2 + \frac{1}{2}\sum_{ij}\frac{1}{r_{ij}} - \sum_{in}\frac{Z_n}{r_{ni}} + \frac{1}{2}\sum_{nm}\frac{Z_nZ_m}{R_{nm}} \qquad\qquad 21$$

In eq. 21, the indexes n and m stand for the nuclei and the indexes i and j for the electrons. The symbol ∇ denotes the partial differentiation over the nuclear (n) or electronic (i) coordinates. The first two terms in 21 denote the nuclear and electronic kinetic energies and the others are the inter-electron, electron-nuclear, and inter-nuclear potential energies, respectively. The total Schroedinger equations can now be split into two parts: the electronic part:

$$\left(-\sum_i \frac{1}{2}\nabla_i^2 + \frac{1}{2}\sum_{ij}\frac{1}{r_{ij}} - \sum_{in}\frac{Z_n}{r_{ni}} + \frac{1}{2}\sum_{nm}\frac{Z_nZ_m}{R_{nm}}\right)|\Psi_{el}(R,r)\rangle = E_{el}|\Psi_{el}(R,r)\rangle \qquad\qquad 22$$

and the nuclear part:

$$\left(-\sum_n \frac{1}{2M_n}\nabla_n^2 + E_{el}\right)|\Psi_{nuc}(R)\rangle = E_{tot}|\Psi_{nuc}(R)\rangle \qquad\qquad 23$$

The adiabatic approximation is valid when different PESs are well-separated, but once the surfaces approach each other, the adiabatic approximation breaks down. The surfaces become non-adiabatic and transitions between them are induced by non-adiabatic coupling. The

probability of the nonadiabatic transitions depends on the energy gap between different PESs. The Schroedinger equation for the i-th state now becomes:

$$(-\sum_n \frac{1}{2M_n}\nabla_n^2 + \frac{1}{M_n}C_{ii} + E_{el}^i)|\Psi_{nuc}\rangle + \sum_{j\neq i}[\sum_n \frac{1}{2M_n}(\nabla B_{ij} + B_{ij}\nabla) - C_{ij}]\,|\Psi_{nuc}\rangle =$$

$$= E_{tot}|\Psi_{nuc}\rangle \qquad\qquad 24$$

where B_{ij} is a derivative coupling define as follows:

$$B_{ij} = \langle\Psi_{el}^i|\nabla_n|\Psi_{el}^j\rangle \qquad\qquad 25$$

Note, that matrix B_{ij} is hollow, i.e. the diagonal elements B_{ii} are all equal to zero. C_{ij} is so called non-adiabatic correction:

$$C_{ij} = \langle\Psi_{el}^i|\nabla_n^2|\Psi_{el}^j\rangle \qquad\qquad 26$$

Two adiabatic S-dimensional hypersurfaces corresponding to two electronic states, where S is a number of the vibrational degrees of freedom, can intersect along (S-2)-dimensional manifold, which is called intersection space.[38-40] Each point of the intersection space corresponds to a conical intersection (CI). The existence of a CI means the molecule can move from the excited state to the ground state without emitting a photon. In the process, the energy of the electrons is transferred to the vibrational energy of the nuclei, which then can lead to breakage and/or formation of chemical bonds. Figure 2 represents an example of a CI. X_1 (see equation 25) and X_2 are so-called branching-plane vectors, or derivative coupling and gradient difference. X_2 can be defined as follows:

$$X_2 = \nabla_n\Delta E_{ij} \qquad\qquad 27$$

where index n denotes the i-th normal mode and ΔE_{ij} is an energy difference between the i-th and j-th states. The physical meaning of the derivative coupling and gradient difference vectors is that they show the quickest way to change an electron structure and the quickest way from the

degeneracy, respectively. From a chemical point of view, the displacement along any of them will lead to the formation of different products of a reaction. Upon reaching the conical intersection, the wave packet is being split: one part continues to move on the same state, and the
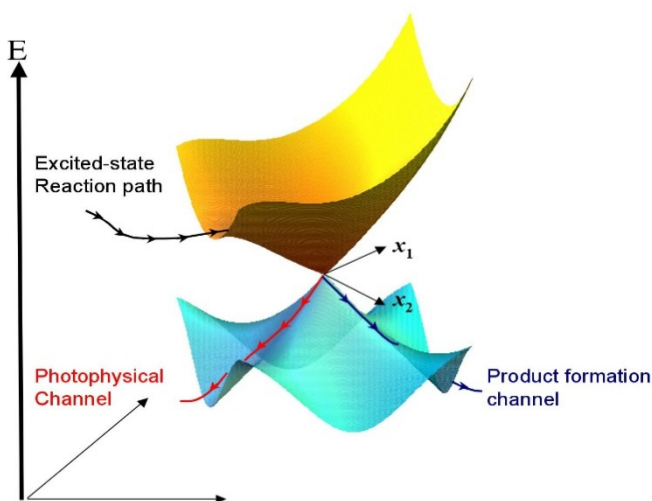
Figure 1.2. The example of a conical intersection.[41]

other propagates on another state, which may further lead to different processes such as dissociation or isomerization. Conical intersections play an important role in the photochemistry because they provide an efficient pathway for non-radiative decay of the excited states.[42-44]

The CI optimization in terms of finding the CI at the minimum energy (minimum-energy CI or MECI) is not a trivial task, because the potential energy gradients on both electronic states are, in principle, non-zero. Instead, the gradient of the intersection seam is used. So, we can formulate the conditions of the minimum energy conical intersections (MECI):[45-49]

$$\Delta E_{ij} = 0 \qquad\qquad 28$$

Condition of the degeneracy of the i-th and j-th states and

$$g_{ij} = 0 \qquad\qquad 29$$

are minimum condition. The operator of projection into the intersection space can be described

as:

$$\hat{P} = \hat{I} - X_1 X_1^T - X_2 X_2^T \qquad\qquad 30$$

I is an identity operator, and X_1, X_2 are the gradient difference and derivative coupling vectors.

Now, the intersection seam gradient can be easily expressed in terms of P:

$$g_{ij} = \hat{P}\frac{E_1}{\partial q} = \hat{P}\frac{E_2}{\partial q} \qquad\qquad 31$$

Nevertheless, finding a MECI is often impractical, because a photochemical reaction may proceed through any point on intersection seam they can reach, so the CIs, obtained from the minimum energy reaction path computation or excited-state molecular dynamics simulation are more important in the photochemistry.

Natural resonance theory

Natural resonance theory[50-54] (NRT) is a relatively new quantum-chemical method, which is based on the first-order density matrix formalism and natural bond orbitals (NBO). The variational NRT results in the representation of the full density matrix as a resonance-weighted linear combination of the reduced density matrices, where each of them corresponds to the "pure" resonance structure. Let us consider the resonance on the "classical" example of benzene molecule:
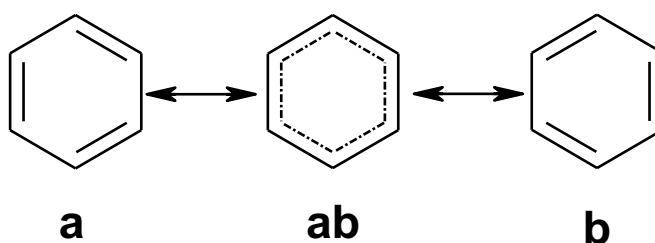
Scheme 1.1. Resonance in benzene molecule

As a matter of fact, the structures **a** and **b** of Scheme 1 are equivalent, but they do not represent reality due to the instantaneous electron flow because of the partial ⇌-orbital overlap. As a result, the real structure of benzene is **ab** with six equalized bonds of 1.5 order. Using the density matrix language, this can be written as

$$D_{ab} = \frac{1}{2}D_a + \frac{1}{2}D_b \qquad\qquad 32$$

where D_{ab} is the full density matrix of a system and D_a and D_b are the "pure" density matrices of the corresponding "pure" resonance structures. Indeed, one can build more than just two resonance forms for benzene, see Scheme 1.2:
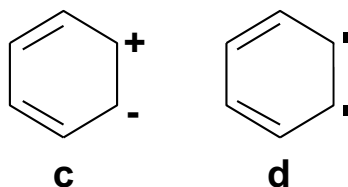
Scheme 1.2. Anionic and diradical forms of benzene

but the their relative weights are insignificant and we can neglect them.

In general, the natural resonance theory can be derived from the basic principles of quantum mechanics. It is a matter of fact, the total wavefunction is a superposition of all possible states of a system:

$$|\Psi\rangle = \sum_i c_i |\Psi_i\rangle \qquad\qquad 33$$

where each of the functions $|\Psi_i\rangle$ denotes the pure i-th state (in this case, the resonance structure). Nevertheless, it is more convenient to apply the density matrix formalism,[55], so that:

$$D = |\Psi\rangle\langle\Psi| = \sum_i |c_i|^2 |\Psi_i\rangle\langle\Psi_i| = \sum_i p_i D_i \qquad\qquad 34$$

where D is a total density matrix, and D_i is a density matrix of the i-th resonance structure, corresponding to the localized (idealized) electron distribution. The density matrix is Hermitian and positively defined, and the coefficients p_i at D_i satisfy the normalization condition:

$$\sum_i p_i = 1 \qquad\qquad 35$$

The trace of density matrix (SpD, sum of diagonal elements) equals to the number of electrons. Moreover it is clear that:

$$SpD = SpD_1 = SpD_2 = \cdots = SpD_i = N \qquad\qquad 36$$

The NRT procedure is based on various redistribution of electron density within the space of valence orbitals. Graphically it can be represented as shown on Scheme 1.3:
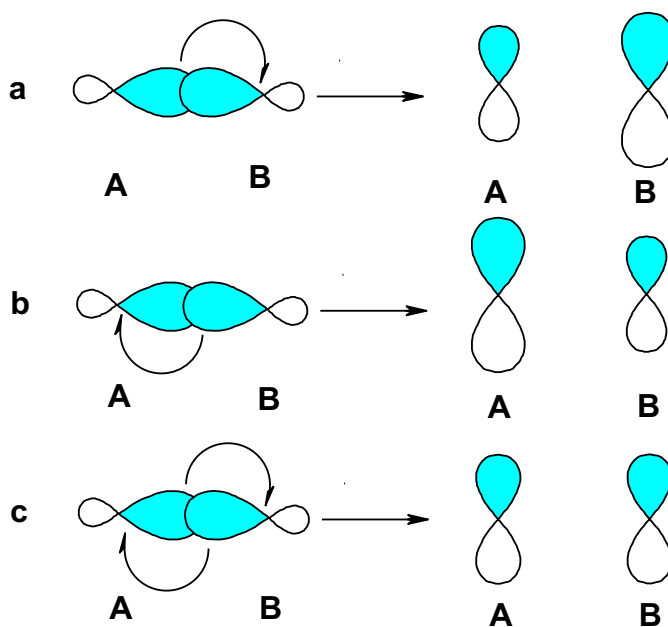
Scheme 1.3. Principle of the NRT algorithm.

Let us consider the covalent diatomic molecule A-B. Cases **a** and **b** of the Scheme 3 represent the localization of the σ_{AB} electron pair on the B and A atoms respectively, which leads to the formation of the limiting ionic resonance structures: A^+B^- and A^-B^+, respectively. But the

σ_{AB} can be split so that one electron becomes localized on A whereas another one on B, which corresponds to a radical pair $A^\bullet B^\bullet$. So, the total NRT equation will have a form

$$|A\text{-}B\rangle = p_1 |A^+B^-\rangle + p_2 |A^-B^+\rangle + p_3 |A^\bullet B^\bullet\rangle \qquad\qquad 37$$

It must be noted that for the construction of the pure density matrix, only natural orbitals (i.e. orbitals with integer occupation number) are used. Actually, every resonance structure is a limiting case of some averaged density. This can be better explained using the following very general example: let us consider a general case represented by the following occupation number vector[56,57] (An ONV is a way to represent a many-electron wavefunction. Every number of an ONV shows the occupation of certain spin-orbital, and therefore, the ONV can be thought as a set diagonal elements of a density matrix because):

$$|\cdots,1,1,0.95,0.04,0.01,0,0,\cdots\rangle \qquad\qquad 38$$

This particular ONV can be expanded in the weighted combination of three limiting cases:

$$|\cdots,1,1,0.95,0.04,0.01,0,0,\cdots\rangle = 0.95 |\cdots,1,1,1,0,0,0,0,\cdots\rangle + 0.04 |\cdots,1,1,0,1,0,0,0,\cdots\rangle +$$

$$0.01 |\cdots,1,1,0,0,1,0,0,\cdots\rangle \qquad\qquad 39$$

After all possible localized resonance structures defined, the weighting coefficients p_i are optimized by minimization of the variational functional:

$$\varepsilon = \mathop{min}_{\{p_i\}}\{((D - \textstyle\sum_i p_i D_i)^2)^{\frac{1}{2}}\} \qquad\qquad 40$$

Solving equation **40** for p_i and keeping conditions **35** (and **36**) yields the resonance structures and their weights.

Natural resonance theory analysis, as it is implemented in NBO program package,[58] provides a valuable tool for chemists since it yields resonance structures and their weights in the intuitively understanding form via a topo-matrix (the matrix, which shows the atomic connectivity and lone-pairs). Nevertheless, NRT must be used carefully with many-body

perturbation theory (MPn) and its derivatives, such as multireference perturbation theory (e.g. CASPT2 and other MRPTn), or configuration interaction/coupled cluster with perturbative treatment of high order excitations (CISD(T), CCSDT[Q], etc.) because these methods use an approximate density, which does not perfectly reproduce the N-particle wavefunction and may end up with "unphysical" population, such as more than one or less than zero electron on a spin-orbital, which violates the Pauli exclusion principle.

References

[1] Haile, J. M. *Molecular dynamics simulation*; Wiley: New York, 1992.

[2] Allen, M. P.;. Rapaport D. C *The Art of Molecular Dynamics Simulation*, Wiley: New York, 1996.

[3] Allen, M. P.; Tildesley, D. J. *Computer simulation of liquids*, Oxford University Press, 1989.

[4] Verlet, L. *Phys. Rev.* 1967, *159*, 98.

[5] Levesque, D.; Verlet, L. *J. Stat. Phys.* 1993, *72*, 519.

[6] Aquilante, F.; Autschbach, J.; Carlson, R. K.; Chibotaru, L. F.; Delcey, M. G.; De Vico, L.; Galvan, I. F.; Ferre, N.; Frutos, L. M.; Gagliardi, L.; Garavelli, M.; Giussani, A.; Hoyer, C. E.; Li Manni, G.; Lischka, H.; Ma, D.; Malmqvist, P.-Å.; Müller, T.; Nenov, A.; Olivucci, M.; Pedersen, T. B.; Peng, D.; Plasser, F.; Pritchard, B.; Reiher, M.; Rivalta, I.; Schapiro, I.; Segarra-Marti, J.; Stenrup, M.; Truhlar, D. G.; Ungur, L.; Valentini, A.; Vancoillie, S.; Veryazov, V.; Vysotskiy, V. P.; Weingart, O.; Zapata, F.; Lindh, R. *J. Comput. Chem.* **2016**, *37*, 506.

[7] Tully, J. C. *J. Chem. Phys.* **1990**, *93*, 1061.

[8] Tully, J. C. *Faraday Discuss.* **1998**, *110*, 407.

[9] Parandekar, P. V.; Tully, J. C. *J. Chem. Phys.* **2005**, *122*, 094102.

[10] Schmidt, J. R.; Parandekar, P. V.; Tully, J. C. *J. Chem. Phys.* **2008**, *129*, 044104.

[11] Raghavachari, K.; Pople, J. A. *Int. J. Quantum Chem.* 1981, *20*, 1067.

[12] Krishnan, R.; Schlegel, H. B.; Pople, J. A. *J. Chem. Phys.* **1980**, *72*, 4654.

[13] Szabo, A.; Ostlund, N. S. *Modern Quantum Chemistry: Introduction to Advanced Electronic Structure Theory*; Macmillan Publishing Co., Inc.: New York, 1982.

[14] Roos, B. O. *Adv. Chem. Phys.* 1987, *69*, 399.

[15] Hirao, K. *Chem. Phys. Lett*. **1992**, *190*, 374.

[16] Hirao, K. Int. *J. Quantum Chem*. **1992**, *S26*, 517.

[17] Hirao, K.; Nakano, H.; Hashimoto, T. *Chem. Phys. Lett*. **1995**, *235*, 430.

[18] Choe, Y.-K.; Nakao, Y.; Hirao, H. *J. Chem. Phys*. **2001**, *115*, 621.

[19] Nakao, Y.; Choe, Y.-K.; Nakayama, K.; Hirao, K. *Mol. Phys*. **2002**, *100*, 729.

[20] Finley, J.; Malmqvist, P. Å.; Roos, B. O.; Serrano-Andrés, L. *Chem. Phys. Lett*. **1998**, *288*, 299.

[21] Granovsky, A. A. *J. Chem. Phys*. **2011**, *134*, 214113.

[22] Angeli, C.; Cimiraglia, R.; Evangelisti, S.; Leininger, T.; Malrieu, J.-P. *J. Chem. Phys*. **2001**, *114*, 10252.

[23] Angeli, C.; Cimiraglia, R.; Malrieu, J.-P. *Chem. Phys. Lett*. **2001**, *350*, 297.

[24] Angeli, C.; Cimiraglia, R.; Malrieu, J.-P. *J. Chem. Phys*. **2002**, *117*, 9138.

[25] Roca-Sanjuan, D.; Aquilante, F.; Lindh, R. *Adv. Rev.* **2012**, *2*, 585.

[26] MacLeod, M. K.; Shiozaki, T. *J. Chem. Phys*. **2015**, *142*, 051103.

[27] Barone, V.; Cossi, M. *J. Phys. Chem. A* **1998**, *102*, 1995.

[28] Cossi, M.; Rega, N.; Scalmani, G.; Barone, V. *J. Comput. Chem*. **2003**, *24*, 669.

[29] Cances, E.; Mennucci, B.; Tomasi, J. *J. Chem. Phys*. **1997**, *107*, 3032.

[30] Cances, E.; Mennucci, B. *J. Math. Chem*. **1998**, *23*, 309.

[31] *Lomize, A. L.; Pogozheva, I. D.; Lomize, M. A.; Mosberg, H. I. Prot. Science **2006**, 15, 1318.*

[32] Schaefer, M.; van Vlijmen, H. W.; Karplus, M. *Adv. Prot. Chem.* **1998**, *51*. 1.

[33] Warshel, A.; Levitt, M. J. Mol. Biol. 1976, 103, 227.

[34] Singh, U. C.; Kollman, P. A. *J. Comput. Chem*. **1986**, *7* (6) 718.

[35] Field, M. J.; Bash, P. A.; Karplus, M. *J. Comput. Chem*. **1990**, *11* (6) 700.

[36] Maseras, F.; Morokuma, K. *J. Comput. Chem*. **1995**, *16* (9) 1170.

[37] Friesner, R. A.; Guallar, V. *Annu. Rev. Phys. Chem*. **2005**, *56*, 389.

[38] von Neumann, J. W. Phys. Z 1929, 30, 467.

[39] Zerner, C. Proc. R. Soc. A 1932, 137 (833) 696.

[40] Teller, E. J. Phys. Chem. 1937, 41, 109.

[41] Boggio-Pasqua, M.; Paterson, M. J.; Robb, M. A.; Blancafort, L.; Anthony, D. D. *J. Phys. Chem. A* **2005**, *109*, 7527.

[42] Zimmerman, H. E. *J. Am. Chem. Soc*. **1966**, *88*, 2.

[43] Michl, J. *Mol. Photochem*. **1972**, 4.

[44] Atchity, G.; Xantheas, S.; Ruedenberg, K. *J. Chem. Phys*. **1991**, *95*, 1862.

[45] Domcke, W.; Yarkony, D. R.; Koppel, H. *Conical Intersections: Electronic Structure, Dynamics & Spectroscopy*; World Scientific Publishing Co.: Singapore, 2004.

[46] Yarkony, D. R. *J. Chem. Phys*. **1990**, *92*, 2457.

[47] Yarkony, D. R. *Rev. Mod. Phys*. **1996**, *68*, 985.

[48] Yarkony, D. R. *J. Chem. Phys*. **2005**, *123*, 204101.

[49] Redmon, L. T. *Phys. Rev. A* **1982**, *25*, 2453.

[50] Pauling, L. *The Nature of the Chemical Bond*, 3rd ed.; Cornell University: Ithaca, NY, 1960.

[51] Wheland, G. W. *Resonance in Organic Chemistry*; Wiley: New York, 1955.

[52] Glendening, E. D.; Weinhold, F. *J. Comput. Chem.* **1998**, *19*, 593.

[53] Glendening, E. D.; Weinhold, F. *J. Comput. Chem.* **1998**, *19*, 610.

[54] Glendening, E. D.; Badenhoop, J. K.; Weinhold, F. *J. Comput. Chem.* **1998**, *19*, 628.

[55] Dahl, J. P. *Introduction to the Quantum World of Atoms And Molecules*; World Scientific Publishing Co.: Singapore, 2001.

[56] Fock, V. A. *Z. Phys.* **1932**, *75*, 622-647.

[57] Reed, M. C.; Simon, B. *Methods of Modern Mathematical Physics*, Vol II; Academic Press 1975.

[58] Glendening, E. D.; Landis, C. R.; Weinhold, F. *J. Comput. Chem.* **2013**, *34*, 1429.

CHAPTER 2: CONNECTING GAS AND LIQUID PHASE PHOTOCHEMICAL DYNAMICS:

AN UNEXPECTED PATHWAY OF DIIODOMETHANE PHOTOISOMERIZATION

Abstract

Photochemical processes play an important role in Nature, from chemical reactions of photochemically active small molecules in the atmosphere to the chemical reactivity of photosynthetic units. All these processes comprise the same elementary steps: an absorption event leading to the population of an excited electronic state, nuclear motion in the Frank-Condon (FC) region on the initially populated potential energy surface (PES) corresponding to the excited state, energy redistribution and flow, structural rearrangement, formation of reaction intermediates, and then, reaction products. One of the interesting objects for photodynamical studies is the polyhalomethane series, where CH_2I_2 serves as a typical representative. Polyhalomethane molecules play an important role in UV photolytic atmospheric processes, e.g. ozone layer decomposition, where the distribution of the internal energy in the fragments formed following the photolysis affects their chemical reactivity. Therefore, it is important to clearly understand the mechanism of their photoinduced transformations.

Literature review

The formation of the isomer, CH_2I-I, after excitation of diiodomethane in solution and condensed phases was previously widely assumed to be due to cage-induced recombination of the initial CH_2I and I radical fragments of the CH_2I_2 UV photodecomposition. However, the ultrafast transient absorption results obtained by our research group disproved this assumption. With the improvement of time resolution of the experiment, it became possible to resolve the formation of the isomer is in solution within the first 100 fs after excitation of CH_2I_2. A timescale

such as sub-100 fs is much shorter than a typical time scale for solute-solvent encounters in

solution (200 fs) and does leave the time for the leaving I• radical to reach the cage, bounce

back, and recombine with the remaining CH_2I• fragment to form the CH_2I-I isomer. Therefore,

the sub-100 fs observation of the CH_2I-I product strongly suggests that the isomer formation

occurs via the intramolecular process, the so-called direct photoisomerization
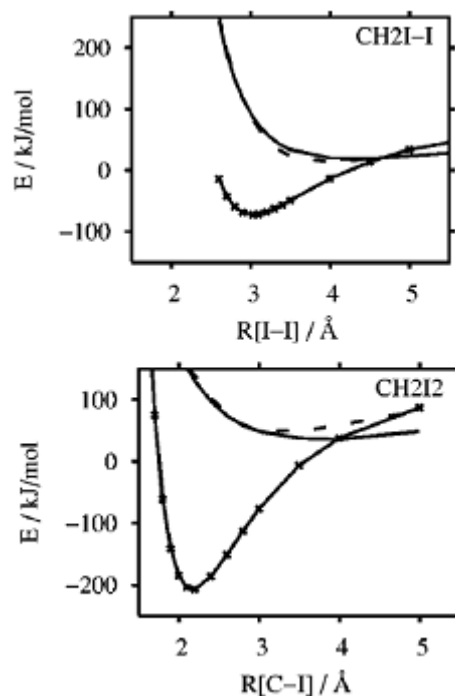
Figure 2.1. The potential energy relaxed scans on the ground and first excited states along I–I
bond in the isomer (top) and C–I bond in the parent molecule (bottom), respectively.

This work gives a mechanistic and dynamic description of the observed direct

isomerzation using modern computational techniques. I employed one of the most accurate

computational method to date, CASPT2 (Complete Active Space Perturbation Theory, 2nd order

energy correction), in semiclassical (with surface hop) molecular dynamics simulations of the

ensemble of 100 vibrationally excited CH_2I_2 molecules promoted to the S_1 surface as a result of

FC (vertical) excitation. The $S_1 \rightarrow S_0$ surface hop occurs at about 35 fs after the excitation event

(at the vicinity of the S_1/S_0 conical intersection) and then, some of trajectories arrive to the isomer species, which have their geometries significantly distorted from that of the equilibrated isomer species.

Thus, based on the ultrafast transient absorption experiments and high-level *ab initio* simulations, we show the existence of the previously unsuspected direct sub-100 fs isomerization of electronically excited CH_2I_2 through a conical intersection. Our computations predict, in agreement with the experimental results, that the recoil from a solvent cage or the presence of solute-solvent interactions is not a necessary requirement for this isomerization reaction to take place.
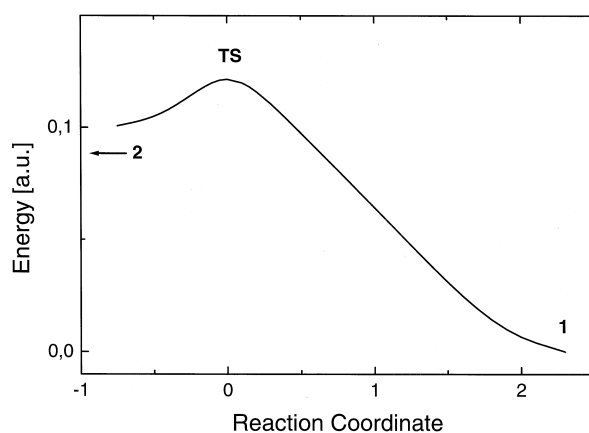
Figure 2.2. The S_0 MEPs from the transition state to the parent (1) and isomer (2) species.

The previous studies[1] show the existence of a conical intersection (CI) that connects the electronically excited CH_2I_2 parent molecule and the $CH_2I\bullet$ and $I\bullet$ radical pair. Odelius and co-workers[2] studied the CH_2I_2 photodissociation path (starting from the FC point o the $^1B_1$ excited state, which is the lowest singlet excited state) in the gas phase and in the acetonitrile cage by using Car-Parrinello molecular dynamics. For the solvation simulations they used a periodic box with a side 15 Å. The photoexcited CH_2I_2 system was described by the restricted open-shell

Kohn-Sham method. The processes of the caged radical pair formation ($CH_2I\bullet$ and $I\bullet$) and their subsequent in-cage recombination into the $CH_2I–I$ isomer were considered. The direct isomerization channel was neither suspected nor observed. The scans of the potential energy surfaces of the first excited and ground states along I–I (for isomer) and C–I (for parent molecule) distances were calculated, Figure 1. Also, the authors concluded that in the case of in-cage radical recombination, the time required for reorientation of the CH_2I fragment to form the I-I bond in the $CH_2I–I$ isomer species must be about 500 fs.

The direct ground state isomerization path shown in Figure 2 was computationally studied by Orel and Kuhn.[3] They discussed the formation of the isomer species via recombination of the nascent radical pair in the condensed phases and concluded that the isomer formation is unlikely because of the shallow isomer ground state minimum. Consequently, the authors concluded that the isomer species most likely play no important role in the UV photochemistry of CH_2I_2.

Later, Lindh et $al.$[4] computed twelve (11-excited) low-lying states of CH_2I_2 by means of the spin-orbit coupled CASPT2 method. Prior to that, the authors carried out spin-free excited-state MS-CASPT2 computation studying the effects of different size of the active space and different basis sets. Scanning the PESs along the C-I bond length they found that the first excited singlet (fifth spin-orbit coupled) state correlates mainly to the $CH_2I\bullet+I\bullet(^2P_{3/2})$ products and that the second singlet excited (eleventh spin-orbit coupled) state dissociates with formation of $CH_2I\bullet+I\bullet*(^2P_{1/2})$. Above, $I(^2P_{3/2})$ and $I(^2P_{1/2})$ correspond to the ground state and spin-orbit excited state, respectively. The direct isomer formation from the excited electronic states of CH_2I_2 was not suspected, and as a result, was not investigated.

```
┌─────────────────────────────┐
│        CASPT2 MEP           │
└─────────────────────────────┘
              │
              ▼
┌─────────────────────────────┐
│      CASPT2 Molecular       │
│         Dynamics            │
└─────────────────────────────┘
              │
              ▼
┌─────────────────────────────┐
│       CASPT2 QM/MM          │
│     Molecular Dynamics      │
└─────────────────────────────┘
```
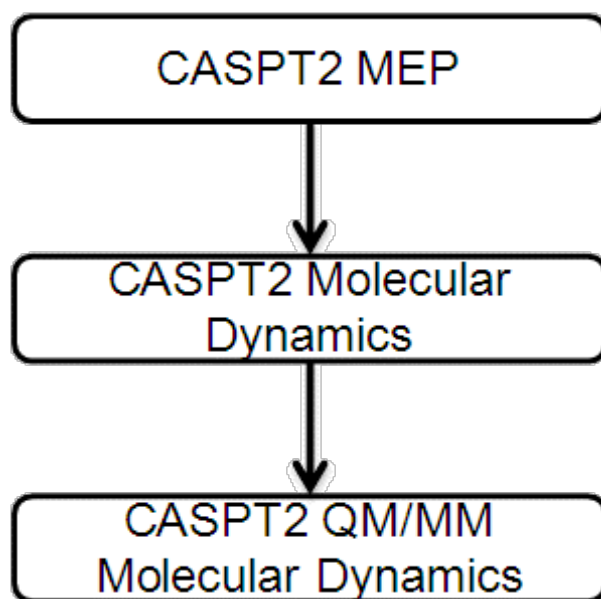
Scheme 2.1. A general methodology of a computational study of polyhalomethane photoisomerization.

New ultrafast transient absorption results obtained in acetonitrile solutions of CH_2I_2 in the Dr. Tarnovsky research group question several major conclusions of the previous studies. Most importantly, the formation of a substantial fraction (~50% of the total quantum yield) of the isomers in the new experiments is found to occur on a timescale of sub-100 fs. This timescale is much shorter than the one would expect for in-cage isomerization of the initial radical pair: on a 100 fs time scale the leaving I• radical has no time to undergo even a single encounter with the solvent cage. Consistent with the impulsive (ballistic) isomerization mechanism, the nascent isomer product species is observed to exhibit the damped coherent oscillations with a 69-cm^{-1} frequency due to vibrational coherence in the C−I−I bending, which presumably is one of the reaction coordinate modes. Furthermore, the recent femtosecond transient absorption experiments in the Tarnovsky research group powered by ~30 fs laser pulses revealed that ultrafast isomerization also takes place upon S_1 excitation of CH_2I_2 in the gas phase.[5] Thus, isomerization of electronically excited CH_2I_2 is direct and unimolecular: the presence of a

solvent cage is not needed for this reaction to occur. The experimental data uniquely suggest that the isomer forms from S_1 CH_2I_2 in the gas phase at ~50 fs, but then undergoes rapid decomposition within the next 70 fs.

Computational methodology

For our studies we have used the methodology, shown in Scheme 2.1. The first step is to compute the excited state minimum energy reaction path[5] in order to verify the possibility of the direct isomerization of diiodomethane. The MEP provides a valuable information about (photo)chemical process, such as the topology of the PES, including those corresponding to excited electronic states, and the existence of local minima or possible surface crossings. The MEP corresponds to the case of overdamped dynamics in which the kinetic energy (KE) is set to zero and a point presentative of the molecule only follows the gradient of potential energy. In other words, the MEP shows an idealized picture of a process. To account for KE, in the next step we plan to run an excited state molecular dynamics[6,7] (MD) simulation in the gas phase. In contrast to the previous method, during the MD simulation the kinetic energy amount is not zero but a finite number, initially determined by the initial conditions (nuclear velocities on the ground electronic state), and this amount is re- distributed over all vibrational modes according to the curvature of the potential. For the MD, it makes sense to simulate the ensemble of the molecules with various initial geometries and atomic velocities. These initial conditions typically, which is the case at hand here, are chosen model the statistical distribution of the internal energy in the starting, equilibrated state across the molecular ensemble. Indeed, in the experiments what were carried out in our research group, we excited and probed not a single molecule, but an ensemble of molecules. The main information one can obtain from the semiclassical MD simulations (non-adiabatic transitions such as surface hops are allowed to

happen) is excited state lifetimes, lifetimes of reaction intermediates and products, distributions of the internal energy in these species, and, in addition, it is possible to evaluate the branching ratios of possible reaction channels (product quantum yields).
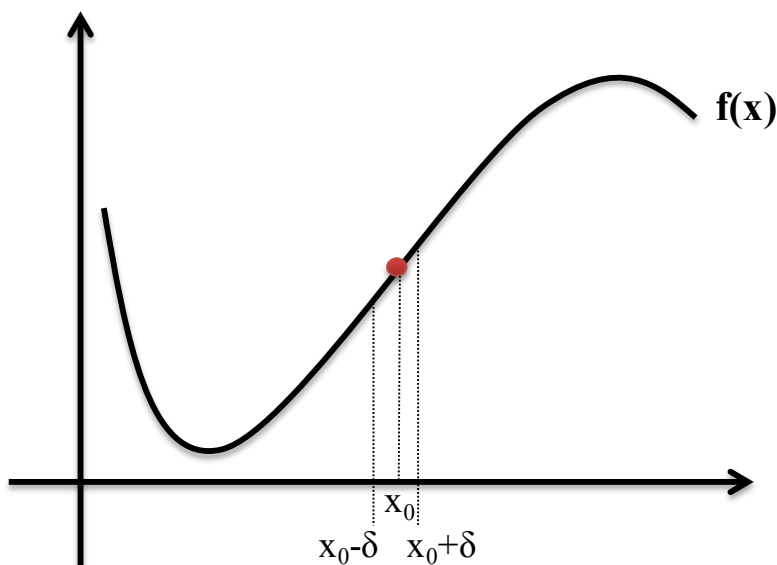
Figure 2.3. A graphical representation of the numerical derivative

The majority of chemical reactions occur in the solution phase. Also, direct isomerization of S_1 CH_2I_2 is reported in the gas as well as in the liquid phases. So, in the last and most advanced step of our modelling semiclassical molecular dynamics simulations should be executed for the CH_2I_2 system in a solvent cage. To achieve this goal, I applied the state-of-the-art technique, a hybrid quantum mechanics/molecular mechanics (QM/MM)[8] approach, see the corresponding section of the Theoretical Background chapter for more details. The QM/MM is available via Molcas-Tinker[9] interface in Molcas 8.1[10] developer version. For the MM part the Amber forcefield parameter set[11] was used, and in the meantime the chromophore is described by an advanced quantum chemical method (see below). The presence of the solvent leads to the electrostatic and van der Waals interactions. These interactions may change qualitative and

quantitative photochemical characteristics of the reaction. They also help to redistribute the vibrational energy over the whole system, which typically leads to the stabilization of reaction intermediate, such as the isomer product species.

For all simulation described above, I used CASPT2,[12,13] see Theoretical Background. Unfortunately, the analytical derivatives are not available for CASPT2 as it is implemented in Molcas program package, therefore, the numerical differentiation must be applied to compute the potential energy gradients. The numerical differentiation utilizes the finite difference method and is illustrated in Figure 2.3. If one needs to compute the gradient of an arbitrary function f(x) at the point of x_0, it is needed to make two steps sufficiently away from x_0 in both directions. Then, using the simple formula, find an approximate value of the first derivative:

$$f'(x_0) \approx \frac{f(x_0+\delta)-f(x_0-\delta)}{2\delta} \qquad\qquad 1$$

The δ-step must not be too large, otherwise the error of the approximated derivative will be large as well, but also the step must not be too small, or the error will be comparable the numerical noise, which is always present in computer simulations, and will cause the failure of a simulation. Despite the fact that numerical differentiation is much simpler than analytical, a program must perform 6N Cartesian (or, 6N-12 internal) single-point energy evaluation, which makes the numerical gradients much more computationally demanding then analytical.

Results and discussion

Since our approach is based on CASSCF[14] wavefunction as a zero-order reference, the active space of the CH_2I_2 system has to be defined. The active space chosen should adequate for the description of the UV photochemistry at hand, so I have chosen 6 lone pairs of iodine and three C-I antibonding orbitals (12 electrons in 9 orbitals, 2520 Slater determinants, see Supporting Information I). For CASPT2, in order to avoid the possible intruder states, the non-standard

imaginary shift[15] of 0.2 Hartree (I Hartree = 27.2107 eV = 627.503 kcal mol⁻¹) was used. The split-valence triple zeta basis set 6-311G**[16,17] with inclusion of d-polarization functions on iodine and carbon, and p-polarization functions on hydrogen have been chosen. For comparison of performance of various methods and basis sets, see the Supporting Information II. The parent and isomer species of CH_2I_2 were optimized using CASPT2 numerical gradients. Then, the numerical vibrational frequencies were computed in order to verify that the obtained structures are the true minima. Both structures and the lowest vibrational frequencies are show in Figure 4.

The isomer molecule is situated in a shallow local minimum, 42.5 kcal/mol higher in energy than the parent species. The I-I bond length is 3.15 Ångstroms (cf. 2.68 Å in molecular iodine[18]), and the carbon atom hybridization is close to sp^2. The adequacy of the chosen active space was verified by reproducing the experimental absorption bands. A comparison of the CASPT2 predicted transitions with the experimentally observed ones is given in Tables 2.1 and 2.2.

Table 2.1. A comparison of experimental and computed vertical excitation transitions (VETs) of the CH_2I_2 parent molecule. The VET energies are given in eV and the VET oscillator strengths are in parentheses.

Transition	CASPT2/6-311G**	Experiment[a]
$S_0 \rightarrow S_1$	4.11(0.0098)	4.19[b]
$S_0 \rightarrow S_2$	4.30(0.017)	4.49[b]
$S_0 \rightarrow S_3$	4.6(0.012)	3.96 (shoulder)[b] 4.91[19]

[a]for more detail, see Table 6S in Supporting Information of ref. [5]; [b] cyclohexane solvent.

Vibration	Frequency, cm⁻¹
I-C-I symm str	118
C-I symm str	477
C-I asymm str	709
I-I-H-H rocking	727
H-C-H twisting	1076
I-C-H-H wagging	1258
H-C-H bending	1424
H-C symm str	3188
H-C asymm str	3280

Vibration	Frequency, cm⁻¹
C-I-I bending	118
I-I str	117
H-C-H twisting	365
I-C-H-H wagging	622
H-C-I bending	713
I-C-H-H rocking	904
H-C-H bending	1424
H-C symm str	3210
H-C asymm str	3356

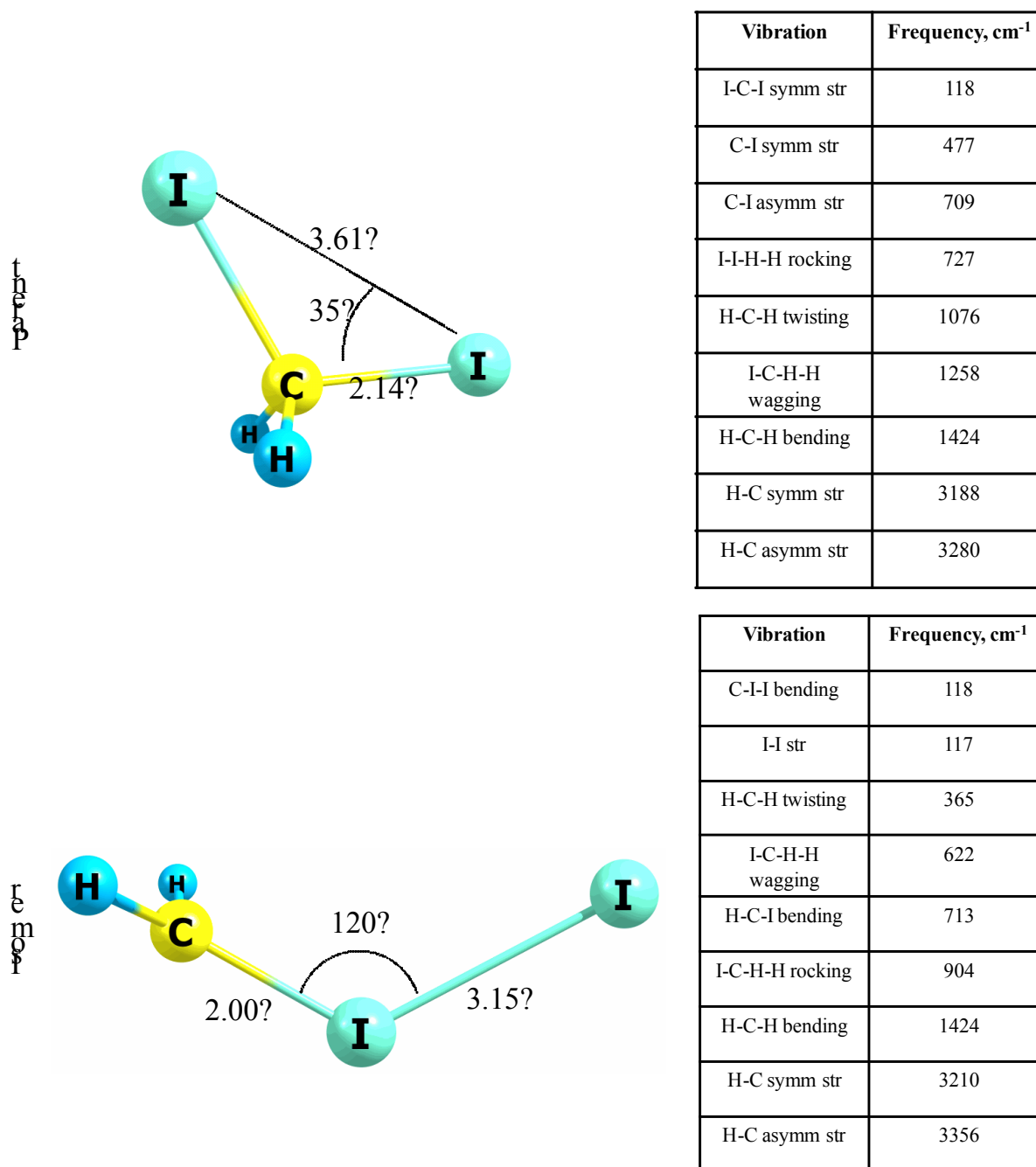**Figure 2.4**. The equilibrium structures of the CH_2I_2 parent and CH_2I-I isomer structures, which correspond to two different minima on the same global ground-state potential energy surface.

Table 2.2. A comparison of experimental and computed vertical excitation transitions (VETs) of the CH_2I-I isomer. The VET energies are given in eV and the oscillator strengths are in parentheses.

Transition	CASPT2/6-311G**	Experiment
$S_0 \rightarrow S_1$	1.2(0.00005)	1.2[a]
$S_0 \rightarrow S_2$	1.3(0.0001)	2.2[b]
$S_0 \rightarrow S_3$	3.2(0.42)	3.21[c,d]

[a]MS-CASPT2 result, ref.[4] supported by the experimental data in acetonitrile solvent, ref. [22]; [b]due to solute-solvent charge transfer.[20-22]; [c]n-hexane solvent. For comparison, this transition is centered at 3.15 eV in CH_3CN;

All transition in the parent molecule can be best characterized as $n \rightarrow \sigma*$ and correspond to HOMO-LUMO, HOMO$_{-1}$-LUMO, and HOMO$_{-2}$-LUMO, respectively. In the isomer, the VET transitions in the order of increasing energy correspond to HOMO-LUMO, HOMO$_{-1}$-LUMO, and HOMO$_{-2}$-LUMO, but can be described as $n \rightarrow \pi*$. The agreement between the computed and experimental transition energies for $S_0 \rightarrow S_2$ excitation is absent, but this transition is likely to be the charge transfer to the solvent.[19-22] Indeed, all high-level *ab initio* methods, namely EOM-CCSD[23-25] (1.4 eV), MR-AQCC[26,27] (1.6 eV), MR-CISD(Q)[28-31] (2.9 eV), fail in the prediction of the second transition.

In order to prove the possibility of the direct excited state isomerization channel, I performed a minimum energy reaction path computation. Since the photoreaction is initiated upon excitation

of the CH_2I_2 molecule into S_1, the MEP was started at the S_1 Frank-Condon point. Because of the
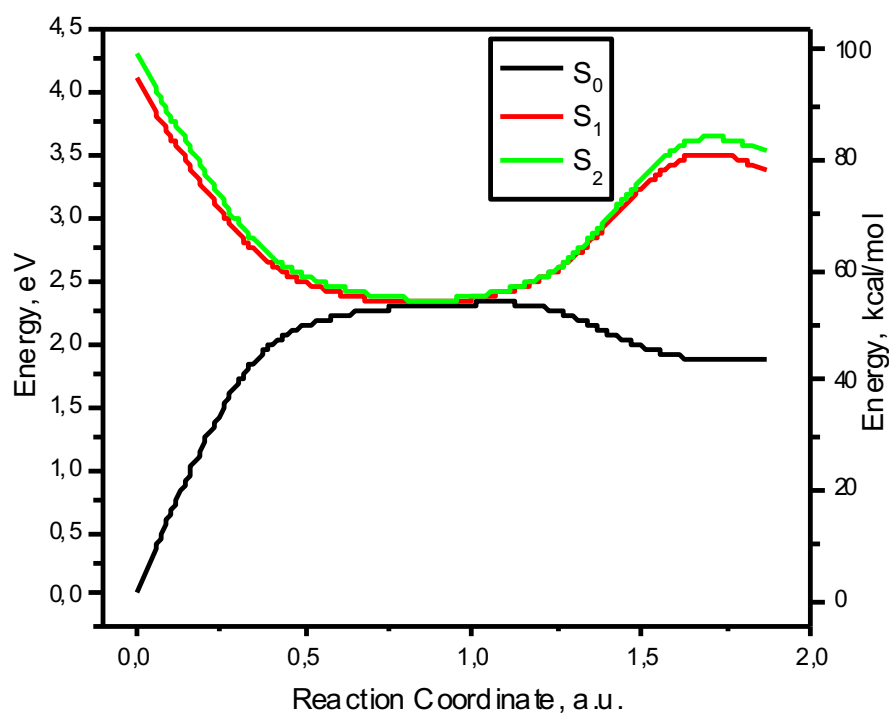
Figure 2.5. The CASPT2 MEP of CH_2I_2

fact that the S_2 state is very close to S_1 and may affect the convergence, I decided to include this

state into the averaging, as a result, the wavefunction I used was averaged over three states (S_0,

S_1, and S_2). The computed MEP (see Figure 2.5) steeply descends to a flatter part of the S_1 PES,

on which a S_1/S_0 conical intersection was found. At the CI, the molecular geometry is found to

be distorted mainly along the I-I distance and the C-I-I angle, which are the major contributors

into the reaction coordinate from the S_1 FC to the CI. The MEP continued (after the CI) on the

ground state ends in a minimum corresponding to the CH_2I-I isomer. A conical intersection

located in a photochemical reaction path at much lower energy than that of the FC point is

energetically accessible. The CI in Fig. 5 is located at lower energy than that of the S_1 FC point,

which provides evidence that isomerization of S_1 CH_2I_2 may occur directly by passage through this energetically accessible CI. The major geometrical changes along the reaction coordinate from S_1 to the CH_2I-I isomer minimum consist of an opening of the C–I–I angle, accompanied by a decrease of the I–I

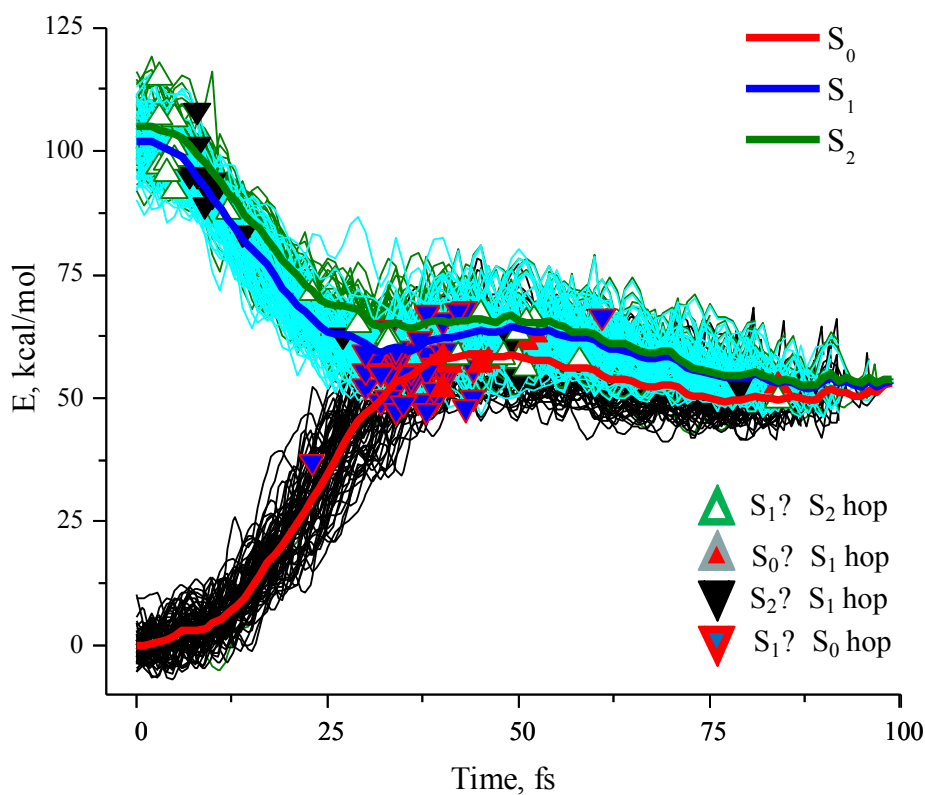**Figure 2.6**. The potential energy profile along the 96 CASPT2 semiclassical trajectories.

distance. As was previously mentioned, the MEP computation provides the description of a chemical reaction at zeroth kinetic energy approximation. For the deeper understanding of the observed phenomena I performed an excited-state quasi-classical molecular dynamics simulations described below.

For excited-state quasi-classical MD simulations, first, 100 initial conditions (molecular geometries and mass-weighted atomic velocities) were generated in Gaussian 09[33] program package, using thermal sampling procedure at the MP2/6-311G** level of theory at temperature of 300 K. The Møller-Plesset perturbation theory[33] was used for generating the initial conditions because the energies and geometries, obtained by MP2, are computationally inexpensive, but close to those obtained by CASPT2. The non-adiabatic surface hopping was taken into account according to Tully[34] Assuming that during an absorption event the initial velocities and geometries do not change, they are used to initiate molecular dynamics at the FC point on the S_1
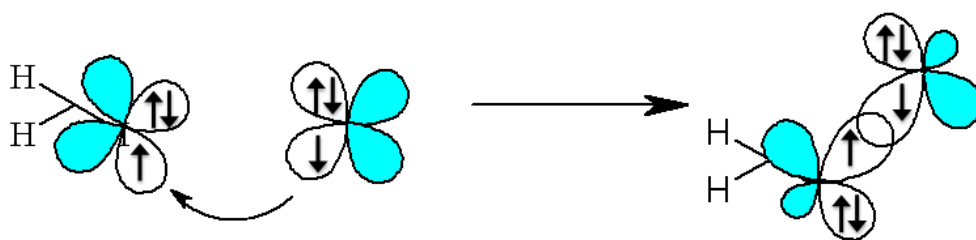
Figure 2.7. A schematic representation of the orbital interaction during the reaction $CH_2I\bullet + I\bullet \rightarrow CH_2I\text{-}I$

of this simulation are presented in Figure 6. The molecular dynamics shows that the trajectory initially propagates on the S_1 state and experiences frequent back and forth $S_1 \leftrightarrow S_2$ surface hops within the first 35 fs. At about 37 fs, the trajectories arrive to the vicinity of the S_1/S_0 CI, where the majority of the trajectories switches to the ground electronic state. After $S_1 \rightarrow S_0$ surface hops, the trajectories qualitatively branch into two fractions. A major fraction (83%) shows either a simple radical dissociation ($CH_2I\bullet$ and $I\bullet$), which amounts to 6%, and the behavior intermediate between direct dissociation and direct isomerization, which amounts to 77%. The remaining, substantial fraction (17%) clearly demonstrates the transient passage through the "isomer valley", which corresponds to a highly vibrationally excited $CH_2I\text{-}I$ with the geometry distorted

in comparison with the equilibrium isomer structure. Not a single trajectory showed the recovery of the parent molecule. The conservation of the total energy is necessary condition for the trajectory to have the physical meaning. As it can be seen in Figure S2.3, Supporting Information, all 96 trajectories shown in Figure 2.6 have their total energy conserved, thus obeying the energy conservation law.

The distinction between "isomer" and "radical pair" is not as straightforward as one might think. The first way, which is a stricter criterion, is to see where the S_1/S_0 energy degeneracy breaks out. This comes from the fact that the electronic nature of the S_1 and S_2 states is due to the $n_I \rightarrow \pi^*_{C-I}$ transitions. Let's consider the $CH_2I\bullet$ and $I\bullet$ radical pair at the infinitely large separation distance. The iodine atom has 7 electrons, distributed over three p orbitals, so its ground state can be described as $p_x^2 p_y^2 p_z^1$. But it is a matter of fact that in the absence of external interactions (e.g, electric/magnetic field of a neighboring atom or a group of atoms) all these orbital are degenerate. Therefore, we can write two more combinations: $p_x^2 p_y^1 p_z^2$ and $p_x^1 p_y^2 p_z^2$. Overall, the ground state of iodine atom is triply degenerate. Now, if this iodine atom approaches the $CH_2I\bullet$ fragment to the interaction distance, one of its previously-degenerate p orbitals (e.g., p_x) overlaps with the p orbital of the iodine of $CH_2I\bullet$, and, as a result, the S_1/S_0 degeneracy of the whole system breaks down.

The energy degeneracy lifting is a necessary condition, but not a sufficient one to state that the CH_2I-I isomer forms during the reaction. To make sure that the nascent product is indeed the isomer, I performed the analysis of the geometrical changes along the trajectories. Since the parent, radical, and isomer species can be distinguished by the I-I distance and C-I-I angle values, I plotted the evolution of these parameters as a function of time, Figure 8. The region,

where the C-I-I and I-I parameters are within 15% from ones in the equilibrium isomer structure, is highlighted.
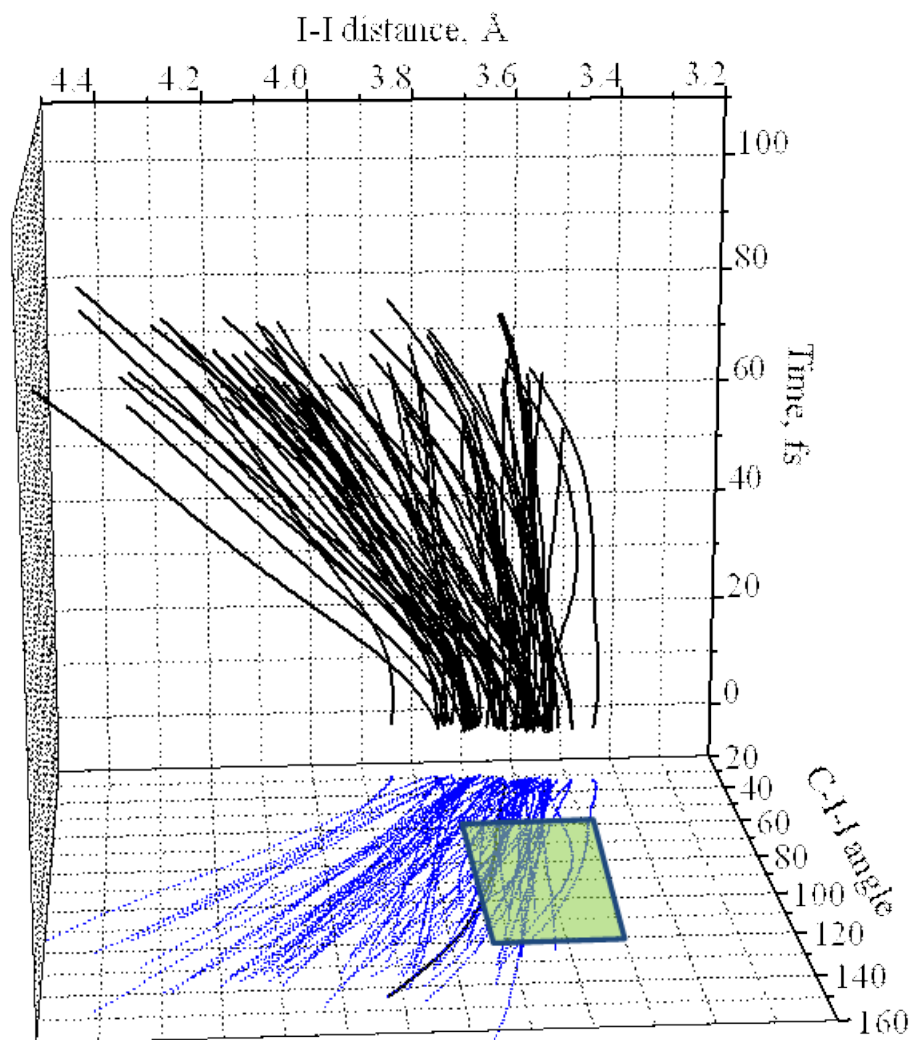
Figure 2.8. An evolution of the I-I distance and the C-I-I angle along MD simulation

By considering the results what were obtained by the analysis of the S_1-S_0 energy gap and the evolution of the molecular structure, one state that the survival time of the isomer product is about 60 fs. The isomer decomposition takes place due to large (~50 kcal/mol) vibrational

energy excess in these species and leads to the formation of I• and internally excited CH$_2$I•

fragments.
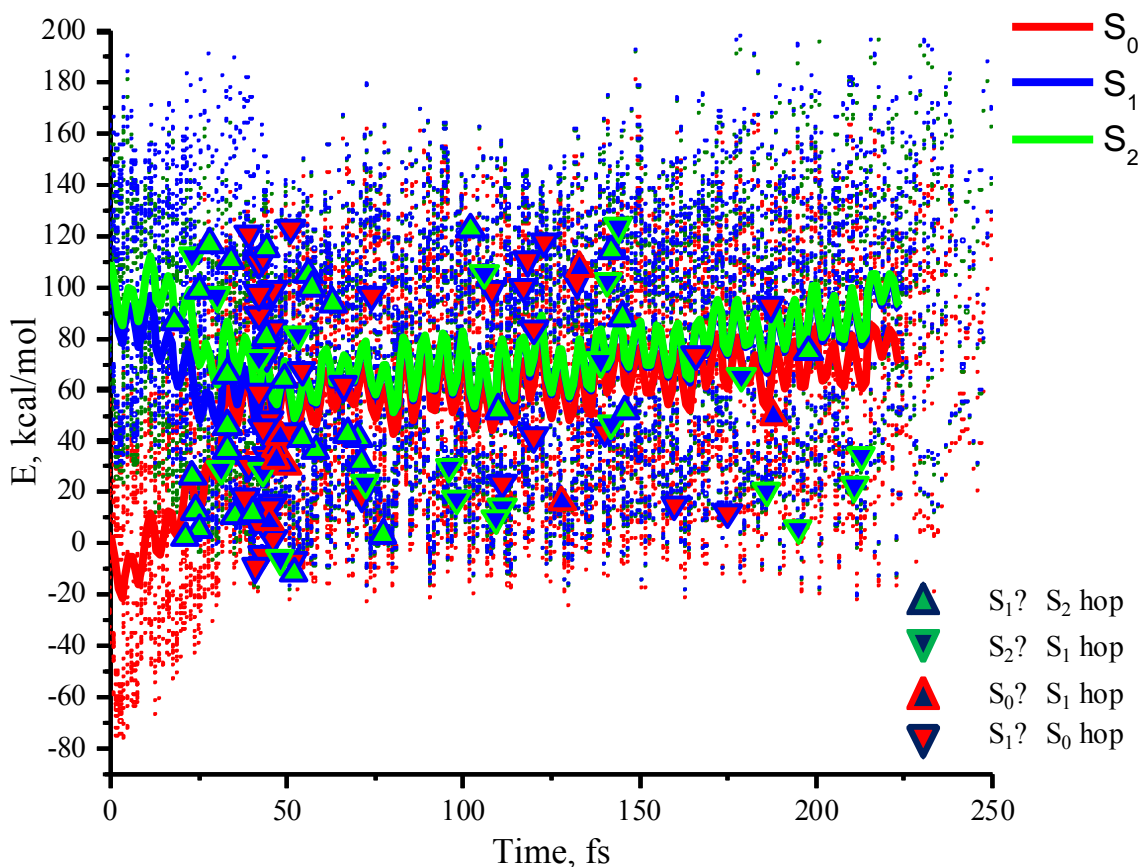
Figure 2.9. The potential energy profile along the 100 CASPT2/6-311G**/Amber
semiclassical trajectories.

The next goal is to simulate the molecular dynamics in the solvent environment. Acetonitrile

solvent is chosen to provide the comparison to the experimental data. As it was previously

mentioned, the continuum solvation models cannot be applied to the dynamic problem such as

CH$_2$I$_2$ direct photoisomerization. Therefore, a hybrid QM/MM approach, which describes the

solvent molecules explicitly, was used. To achieve this goal, I generated a solvent box with

periodic boundary conditions, with a side of 40 Ấ. The box was filled out with 729 acetonitrile

molecules in accordance to the density (0.79 g/cm^3). The entire system was thermalized for 10

nanoseconds at 300 K in Tinker 5.3 program package. Then, the diiodomethane molecule was placed in the middle of the box, and the first three solvent shells were set as "active", i.e. they were available to move. On this new system, I performed a 6-ns molecular dynamic simulation with a frozen CH_2I_2 solute and frozen solvent molecules located outside a 7 Å radius from the CH_2I_2, and every 50 picoseconds the snapshots of the trajectory were saved. Thus, I obtained 100 different cavities, and for each of them I run a 200 fs MD simulation at the MP2/6-311G**/Amber level of theory (this means that the solute is described by MP2 using a 6-311G** basis set, whereas the Amber forcefield is applied to the solvent). The last step is necessary for obtaining the initial velocities on both QM and MM parts of the system. As in the case of the gas-phase MD simulations, the CH_2I_2 molecules in the generated systems were placed in the FC point on the first excited S_1 state and, subsequently, the molecular dynamics was started (see Figure 9). The non-adiabatic surface hops was taken into account according to Tully[34] The technique allowing to use Tully surface hop with QM/MM protocol is available in Molcas 8.1 developer version.

The initial course of the dynamics in the liquid phase is similar to that in the gas phase. Nevertheless, after some time the differences appear. First, the average time of the $S_1{\rightarrow}S_0$ hop is 73 fs in solution (ca. 37 fs in the gas-phase). Second, due to the redistribution of the vibrational energy over the whole "active" QM/MM system (CH_2I_2 and 51 acetonitrile molecules lying within the 7 Å radius), the majority of the initial CH_2I-I isomer molecules does not dissociate anymore. Instead, the nascent CH_2I-I product species form in the geometry that is close to the equilibrium one, and remain stable to the end of simulation (~250 fs). Finally, 6 trajectories pass through the 'parent valley' transiently, and 4 of them remain there up to 250 fs, showing the recovery of the parent ground-state molecule.
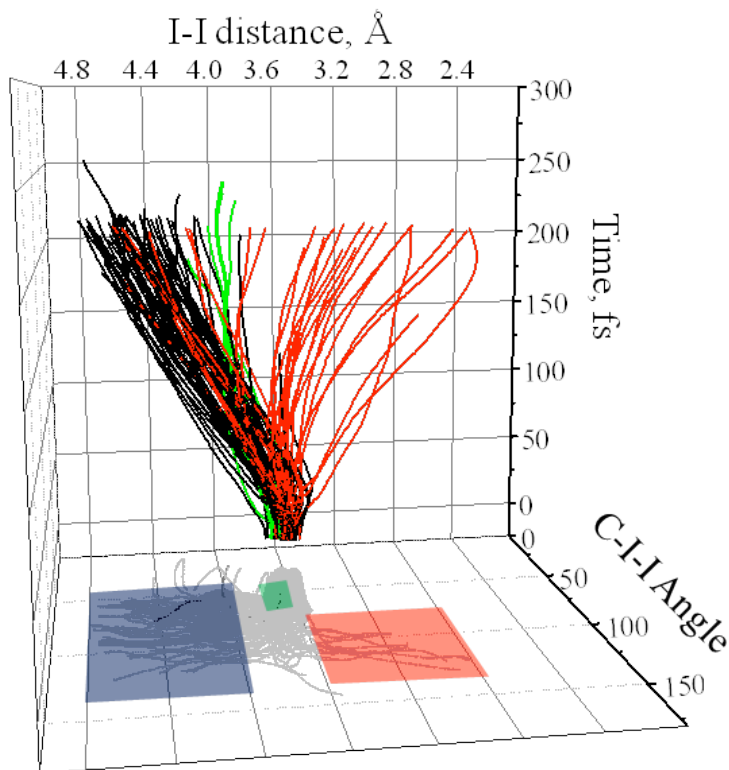
Figure 2.10. An evolution of the I-I distance and C-I-I angle along the 100 of QM/MM trajectories. Trajectories, leading to the isomer, parent, and radical pair depicted by the red, green, and black colors respectively.

To carry out the aforementioned analysis, we, similarly to the case of gas-phase MD simulations, distinguished three types of trajectories (parent recovery, radical formation, and formation of isomers). All computed trajectories were assigned to the above types according to the energy degeneracy/geometrical changes they exhibit (see Figure 2.10). The I-I distance and C-I-I angle values distinguish these three different reaction channels, and the ranges of I-I/C-I-I values for a specific aforementioned channel form three distinct I-I/C-I-I areas, Figure 2.10. Tracing the isomer I-I/C-I-I area as a function of time, it is clearly seen that the initial isomers are stable on, a least, a 250 fs time scale. Within this time interval, C-H modes of CH_2I-I become vibrationally excited as a result of intramolecular vibrational energy redistribution as well as the CH_3CN

molecules adjacent to CH_2I-I become translationally excited as a result of energy transfer from the solute to the solvent. This leads to energy equilibration and stabilization of the isomer species, and undoubtedly, they can survive a much longer time than 250 fs. In experiments, the equilibrated CH_2I-I species have a 220-ns lifetime in the acetonitrile solution Investigating the decomposition of the equilibrated CH_2I-I species is computationally expensive and is outside the scope of the current study.
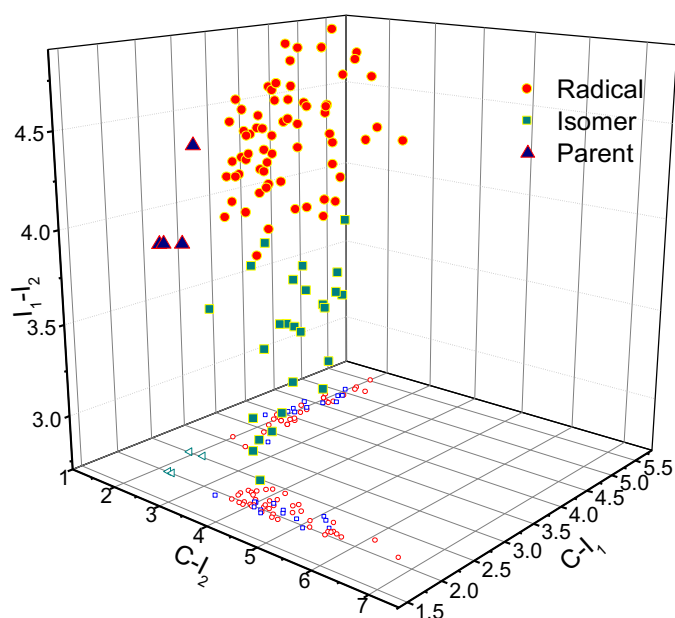
Figure 2.11. Two C-I bond lengths and I-I distance at the last point (~250 fs) of the QM/MM simulation.

Another way to distinguish between different product structures is to look simultaneously at all three distances: $C-I_1$, $C-I_2$, and I_1-I_2 . Indeed, the parent molecule can be characterized by a relatively short length of both C-I bonds (~2 Å) and the I-I distance of ~4 Å. For the radical pair, one of two C-I bonds is broken and the corresponding C-I distance is significantly longer than that the equilibrium parent structure Similarly to the radical pair, in the isomer species, one of the

C-I bonds is substantially elongated, but the I-I distance is relatively short (< 3.6 Å). Figure 2.11 depicts the aforementioned parameters for the last point of the trajectories.

To summarize the results of the QM/MM molecular dynamics simulation, 34 trajectories out of 100 shows the sub-100 fs formation of the CH_2I-I isomer. Eight of them transiently pass through and the remaining 26 reaches the "isomeric" state and remain there until the end of simulation. 62 trajectories go directly to the radical pair and the remaining four show the recovery of the parent molecule.

Conclusion

I showed that the photochemical isomerization path of diiodomethane in gas phase and in solution is direct and mediated by energetically and dynamically accessible S_1/S_0 conical intersection. High-level computations in the gas phase show the formation of the isomeric species on the sub-100 fs timescale, in complete agreement with the isomerization time scale determined in experiments. These results suggest that the gas-phase conditions do not make any difference to the reaction outcome (formation of the isomer product of direct isomerization), but the presence of the polar solvent environment (CH_3CN) affects the initial, short-time course of the isomerization.

According to semiclassical molecular dynamic simulations, as the molecule leaves the S_1 FC region, the ensuing dynamics is initially governed by a steep S_1 surface. Following the passage of the system through CI, the dynamics slows down on a fairly flat S_0 surface. Specifically, the molecule undergoes the $S_1 \rightarrow S_0$ surface hop at the vicinity of the CI at ~ 37 fs in the gas phase and ~73 fs in the CH_3CN solution, and ~ 10 fs later, the I–I bond of the CH_2I-I isomer species is formed. Thus, I present the first solid proof of (a) that the photoisomerization of CH_2I_2 is direct, and (b) the presence or absence of the solvent cage around an CH_2I-I

isomerizing changes the initial course of the reaction, but does not does change the reaction outcome.

References

1] El-Khoury, P. Z.; Tarnovsky, A. N.; Schapiro, I.; Ryazantsev, M. N.; Olivucci, M. *J. Phys. Chem. A* **2009**, *113*, 10767.

[2] Odelius, M.; Kadi, M.; Davidsson, J.; Tarnovsky, A. N. *J. Chem. Phys.* **2004**, *121*, 2208-2214.

[3] Orel, A. E.; Kuhn, O. *Chem. Phys. Let*. **1999**, *304*, 285.

[4] Liu, Y. L.; De Vico, L.; Lindh, R.; Fang, W. H. *ChemPhysChem.* **2007**, *8*, 890.

[5] Borin, V. A.; Matveev, S. M.; Budkina, D. S.; El-Khoury, P.-Z.; Tarnovsky, A. N. *PhysChemChemPhys*, Accepted, **2016.**

[6] Alder, B. J.; Wainwright, T. E. *J. Chem. Phys. 1959, 31, 459.*

[7] Rahman, A. *Phys. Rev. A* **1964***, 136,* 405.

[8] Warshel, A.; Levitt, M. *J. Mol. Biol.* **1976***, 103,* 227.

[9] Ponder, J. Tinker, version 6.3 http://dasher.wustl.edu/tinker/

[10] Aquilante, F.; Autschbach, J.; Carlson, R. K.; Chibotaru, L. F.; Delcey, M. G.; De Vico, L.; Galvan, I. F.; Ferre, N.; Frutos, L. M.; Gagliardi, L.; Garavelli, M.; Giussani, A.; Hoyer, C. E.; Li Manni, G.; Lischka, H.; Ma, D.; Malmqvist, P.-Å.; Müller, T.; Nenov, A.; Olivucci, M.; Pedersen, T. B.; Peng, D.; Plasser, F.; Pritchard, B.; Reiher, M.; Rivalta, I.; Schapiro, I.; Segarra-Marti, J.; Stenrup, M.; Truhlar, D. G.; Ungur, L.; Valentini, A.; Vancoillie, S.; Veryazov, V.; Vysotskiy, V. P.; Weingart, O.; Zapata, F.; Lindh, R. *J. Comput. Chem.* 2016, 37, 506.

[11] Cerutti, D. S.; Rice, J. E.; Swope, W. C.; Case, D. A. *J. Phys. Chem*. B **2013**, *117*, 2328.

[12] Andersson, K.; Malmqvist, P.-Å.; Roos, B. O.; Sadlej, A. J.; Wolinski, K. *J. Phys. Chem.***1990**, *94*, 5483.

[13] Andersson, K.; Malmqvist, P.-Å.; Roos, B. O. *J. Chem. Phys.* **1992**, *96*, 1218.

[14] Roos, B. O. *Adv. Chem. Phys.* **1987**, *69*, 399.

[15] Forsberg, N.; Malmqvist, P.-Å. *Chem. Phys. Letters*, **1997**, *274*, 196.

[16] McLean, A. D.; Chandler, G. S. *J. Chem. Phys.* **1980**, *72*, 5639.

[17] Krishnan, B. R.; Binkley, J. S.; Seeger, R.; Pople, J. A. *J. Chem. Phys.* 1980, 72, 650.

[18] Benson, S. W. *J. Chem. Educ.* **1965**, *42*, 502.

[19] Gedanken, A.; Rowe, M. D. *Chem. Phys.* **1979**, *36*, 181.

[20] Maier, G.; Reisenauer, H. P. *Angew. Chem., Int. Ed. Engl.* **1986**, *25*, 819.

[21] Maier, G.; Reisenauer, H. P.; Hu, J.; Schaad, L. J.; Hess, B. A. *J. Am. Chem. Soc.* **1990**, *112*, 5117.

[22] Ueltschi, T. W.; Fischer, S. A.; Edoardo, A.; Tarnovsky, A. N.; Govind, N.; El-Khoury, P. Z.; Hess, W. P. *J. Phys. Chem. A* **2016**, *120*, 556.

[23] Bartlett, R. J.; Musial, M. *Rev. Mod. Phys.* 2007, 79, 291.

[24] Sekino, H.; Bartlett, R. J. *Int. J. Quantum Chem.* 1984, 18, 255.

[25] Stanton, J. F.; Bartlett, R. J. *J. Chem. Phys.* 1993, 98, 7029.

[26] Szalay, P. G.; Bartlett, R. J. Chem. Phys. Lett. **1993**, 214, 481.

[27] Szalay, P. G.; Bartlett, R. J. J. Chem. Phys. **1995**, 103, 3600.

[28] Langhoff, S. R.; Davidson, E. R. Int. J. Quantum Chem. **1974**, 8, 61.

[29] Bruna, P. J.; Peyerimhoff, S. D.; Buenker, R. J. Chem. Phys. Lett. **1981**, 72, 278.

[30] Werner, H.-J.; Knowles, P. J. J. Chem. Phys. **1988**, 89, 5803.

[31] Knowles, P. J.; Werner, H.-J. Theor. Chim. Acta **1992**, 84, 95.

[32] Frisch, M. J.; Trucks, G. W.; Schlegel, H. B.; Scuseria, G. E.; Robb, M. A.; Cheeseman, J. R.; Scalmani, G.; Barone, V.; Mennucci, B.; Petersson, G. A.; Nakatsuji, H.; Caricato, M.; Li, X.; Hratchian, H. P.; Izmaylov, A. F.; Bloino, J.; Zheng, G.; Sonnenberg, J. L.; Hada, M.; Ehara, M.; Toyota, K.; Fukuda, R.; Hasegawa, J.; Ishida, M.; Nakajima, T.; Honda, Y.; Kitao, O.; Nakai, H.; Vreven, T.; Montgomery, J. A., Jr.; Peralta, J. E.; Ogliaro, F.; Bearpark, M.; Heyd, J. J.; Brothers, E.; Kudin, K. N.; Staroverov, V. N.; Kobayashi, R.; Normand, J.; Raghavachari, K.; Rendell, A.; Burant, J. C.; Iyengar, S. S.; Tomasi, J.; Cossi, M.; Rega, N.; Millam, J. M.; Klene, M.; Knox, J. E.; Cross, J. B.; Bakken, V.; Adamo, C.; Jaramillo, J.; Gomperts, R.; Stratmann, R. E.; Yazyev, O.; Austin, A. J.; Cammi, R.; Pomelli, C.; Ochterski, J. W.; Martin, R. L.; Morokuma, K.; Zakrzewski, V. G.; Voth, G. A.; Salvador, P.; Dannenberg, J. J.; Dapprich, S.; Daniels, A. D.; Farkas, Ö.; Foresman, J. B.; Ortiz, J. V.; Cioslowski, J.; Fox, D. J.Gaussian 09, revision A.02; Gaussian Inc.: Wallingford, CT, **2009**.

[33] Møller, C.; Plesset, M. S. *Phys. Rev.*, **1934**, *46*, 618.

[34] Tully, J. C. *J. Chem. Phys.* 1990, 93, 1061.

Supporting Information

HOMO-5, n   HOMO-2, n   LUMO, s *

HOMO-4, n   HOMO-1, n   LUMO+1, s *

HOMO-3, n   HOMO, n   LUMO+2, s *
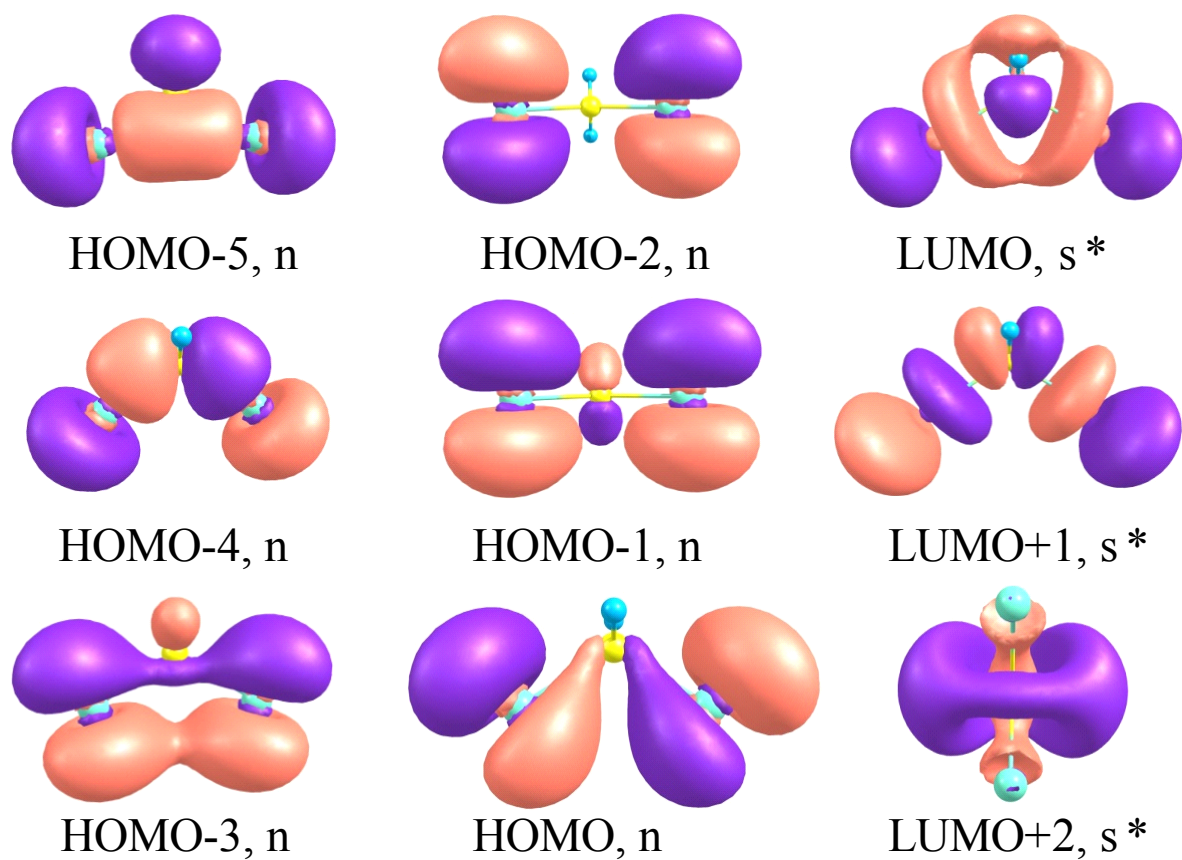
Figure S2.1 The active space orbitals of CH_2I_2 parent molecule
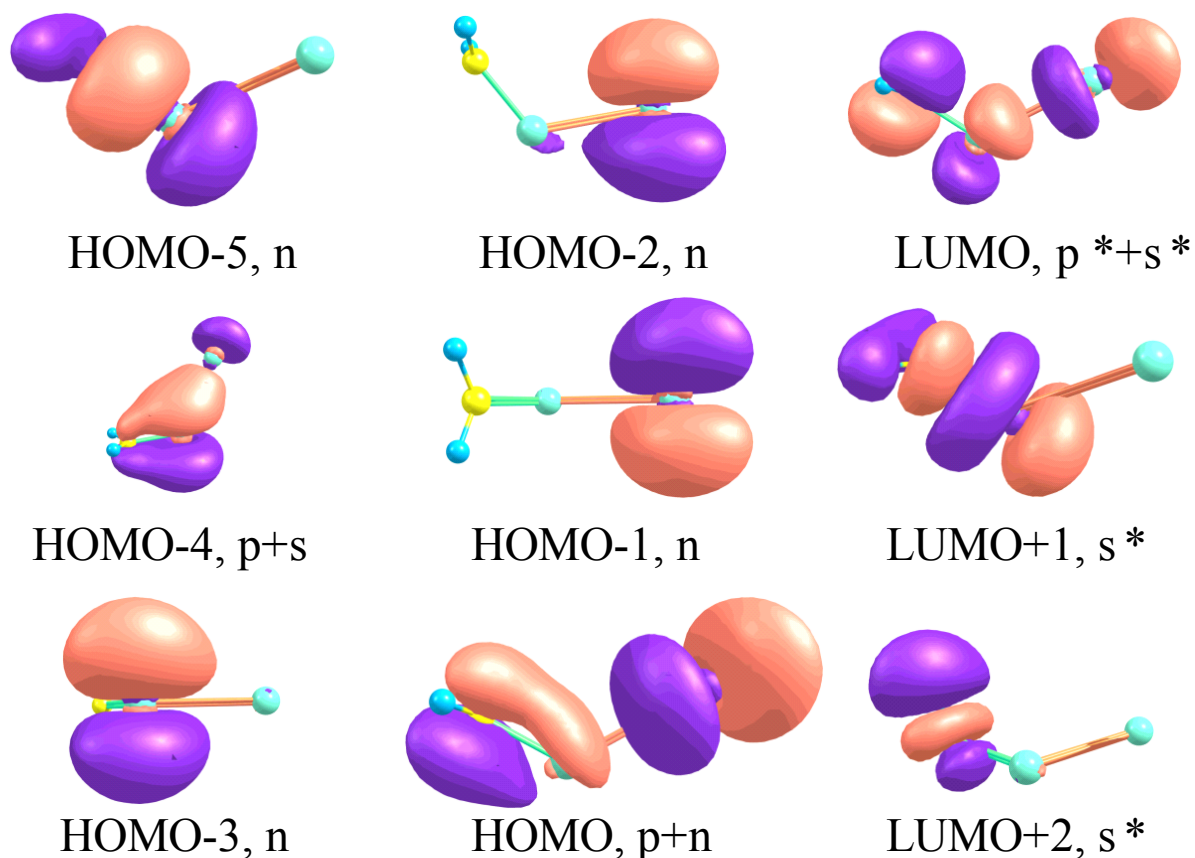
Figure S2.2 The active space orbitals of CH_2I_2 isomer molecule

The active space of parent molecule consists of six lone pairs, and three antibonding σ^*_{C-I} orbitals. The low-lying excited states are governed by the transition from various HOMO's to LUMO. In contrast to parent, the orbitals of the isomer show a complexity, caused by mixing of orbitals of different character: e.g. HOMO-4 and HOMO are formed by interaction of π_{C-I} and σ_{I-I}, and π_{C-I} and n_I orbitals respectively. As well as the aforementioned HOMO's, the LUMO may best be described as a mixture of antibonding π^*_{C-I} and σ^*_{I-I}.

Table S2.1. Performance of various level of theory in appliance to the CH_2I_2 parent molecule

	6-311G**[1]	ANO-RCC-DZVP[2]	ANO-RCC-TZVP[2]	ANO-RCC-QZVP[2]	EOM-CCSD/6-311G**[3]	Experiment[4,5]
C-I, ?	2.14	2.15	2.14	2.14	2.15	2.13
I-I, ?	3.60	3.62	3.54	3.50	3.65	3.52
C-I-I, deg	35.0	32.4	32.9	34.7	32.0	-
VET, eV	4.11, 4.20	4.34, 4.52	4.08, 4.22	4.03, 4.18	4.24, 4.50	4.0, 4.3
Time, min	6	4	13	40	60	

Table S2.1 shows a comparison of the spectroscopic and structural characteristics of the parent molecule, obtained by CASPT2 method, using 6-311G** and ANO-RCC-DZVP − QZVP basis sets and EOM-CCSD/6-311G** with the experimentally observed. The last row gives the average computer time, which is needed to perform a single point energy calculation. This value is important because it shows how demanding a certain computational method is. It must be noted that the first trial of using ANO-RCC-TZVP and QZVP bases failed due to its cost; the values have been obtained after the new Choleski decomposition technique was released in Molcas 8.0 program. The geometry for EOM-CCSD excitation energy calculation has been optimized using CCSD method[6] and Q-Chem 4.2 program package[8].

As it clearly seen, the CASPT2 with 6-311G**, ANO-RCC-TZVP, and ANO-RCC-QZVP better reproduce the experimental data on excitation energies and geometry of the molecule, but the computational cost of the last two bases is too high. Thus, the 6-311G** basis set has been chosen to carry out all simulations.
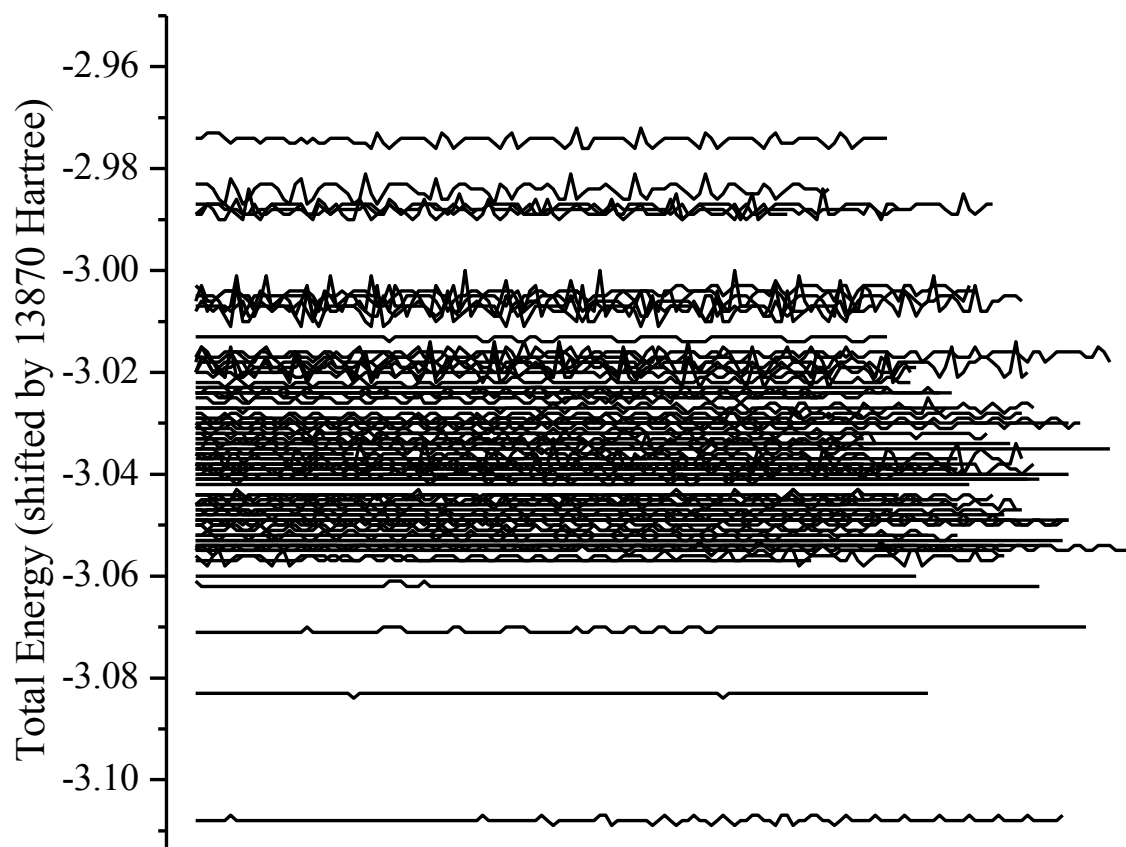
Figure S2.3. Total energy change along the gas-phase CASPT2/6-311G** semiclassical trajectory of CH_2I_2
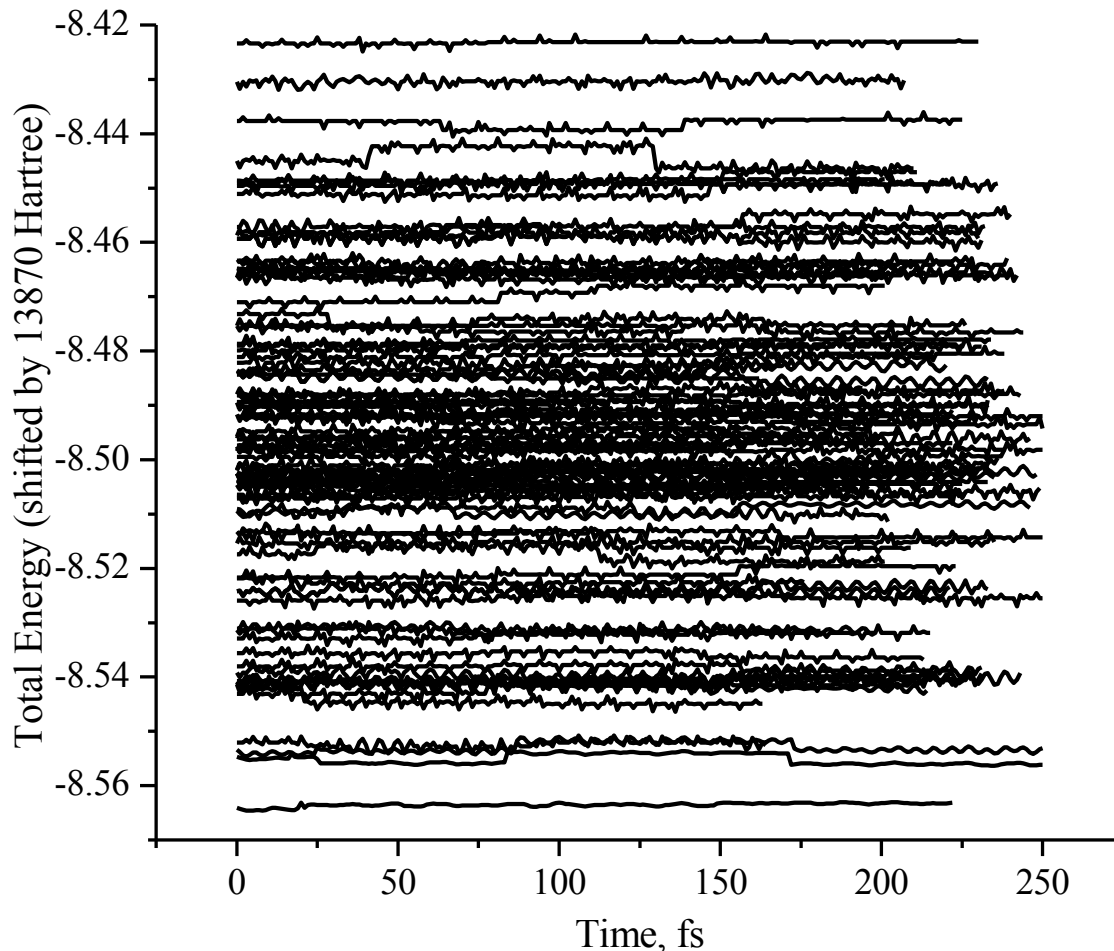
Figure S2.4. Total energy change along the CASPT2/6-311G**/Amber semiclassical trajectory of CH_2I_2

Since the ensembles I have generated are microcanonical (NVE), I paid a special attention to the total energy conservation. **Figures S2.3** and **S2.4** depict the total energy along the gas-phase and QM/MM trajectories respectively. If the energy difference between any of 2 points on trajectory is about the accuracy of CASPT2 method (~2.5 kcal/mol or ~0.005 Hartree)[8], the energy was considered to be conserved. The gas-phase case shows "steps" at the points of surface hops, probably due to the imperfection of the code, which prevents the rescaling of the atomic velocities. Unlike gas-phase, the solvent phase total energy looks more straight because I used a thermostat condition, which rescales the velocities on order to keep the total energy constant.

Table S 2.2 Mulliken charges in ground and excited states of patent molecule

	H_1	H_2	C_1	I_1	I_2
S_0	0.1787	0.1787	-0.4819	0.0622	0.0622
S_1	0.1731	0.1731	-0.4552	0.0902	0.0187
S_2	0.1778	0.1778	-0.4675	0.2007	-0.0886
S_3	0.1772	0.1772	-0.4693	-0.1329	0.2481
S_4	0.1777	0.1777	-0.4819	-0.0059	0.1323
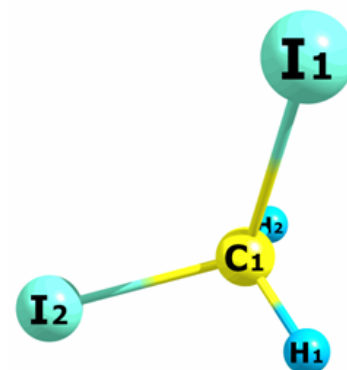
Table S2.3 Mulliken charges in ground and excited states of the isomer molecule

	H_1	H_2	C_1	I_1	I_2
S_0	0.1643	0.1643	-0.3976	-0.2353	0.3044
S_1	0.1646	0.1646	-0.4311	-0.0031	0.1051
S_2	0.1643	0.1643	-0.4275	0.0090	0.0900
S_3	0.1608	0.1608	-0.2550	-0.4329	0.3662
S_4	0.1738	0.1738	-0.5365	-0.5491	0.7380
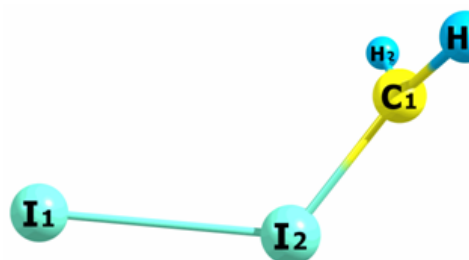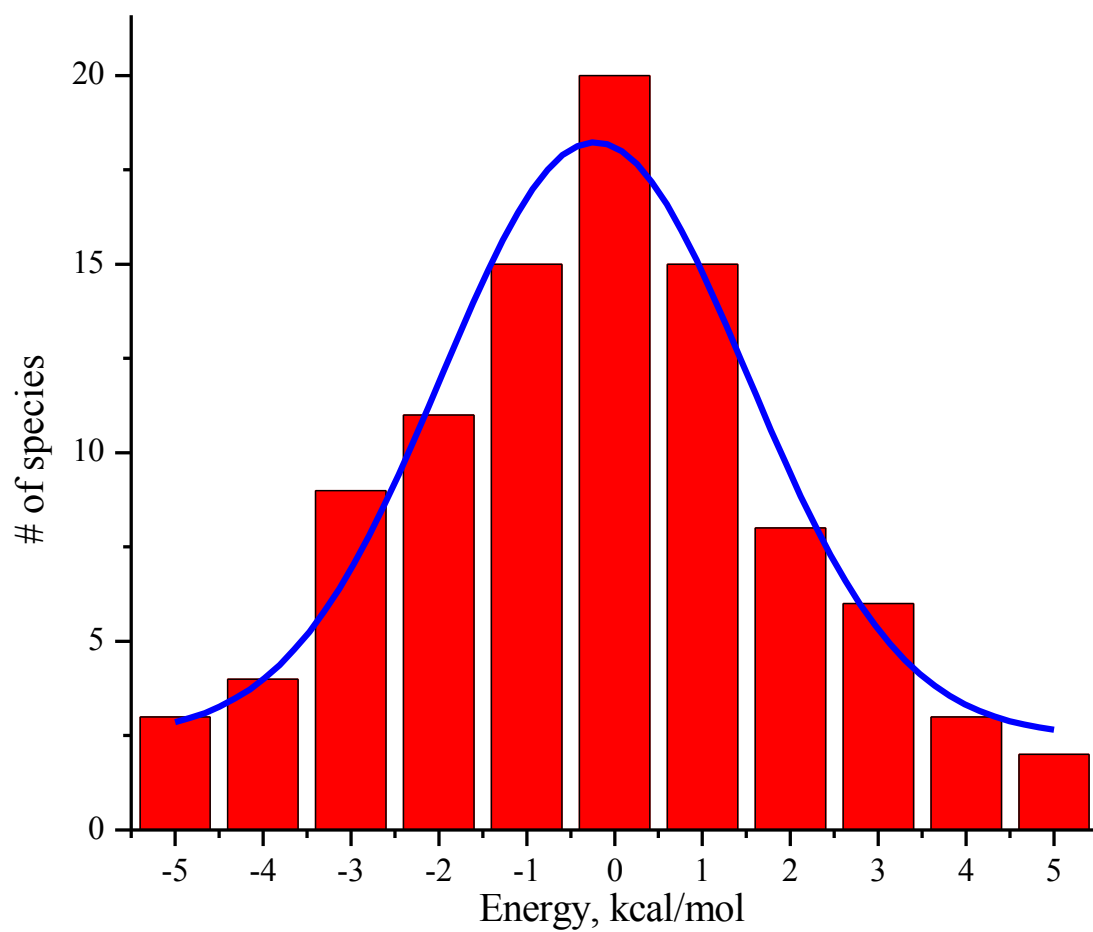
Figure S2.5. A distribution of the gas-phase initial condition (red bars) and exponential fit, represented as number of species vs. its relative energy.
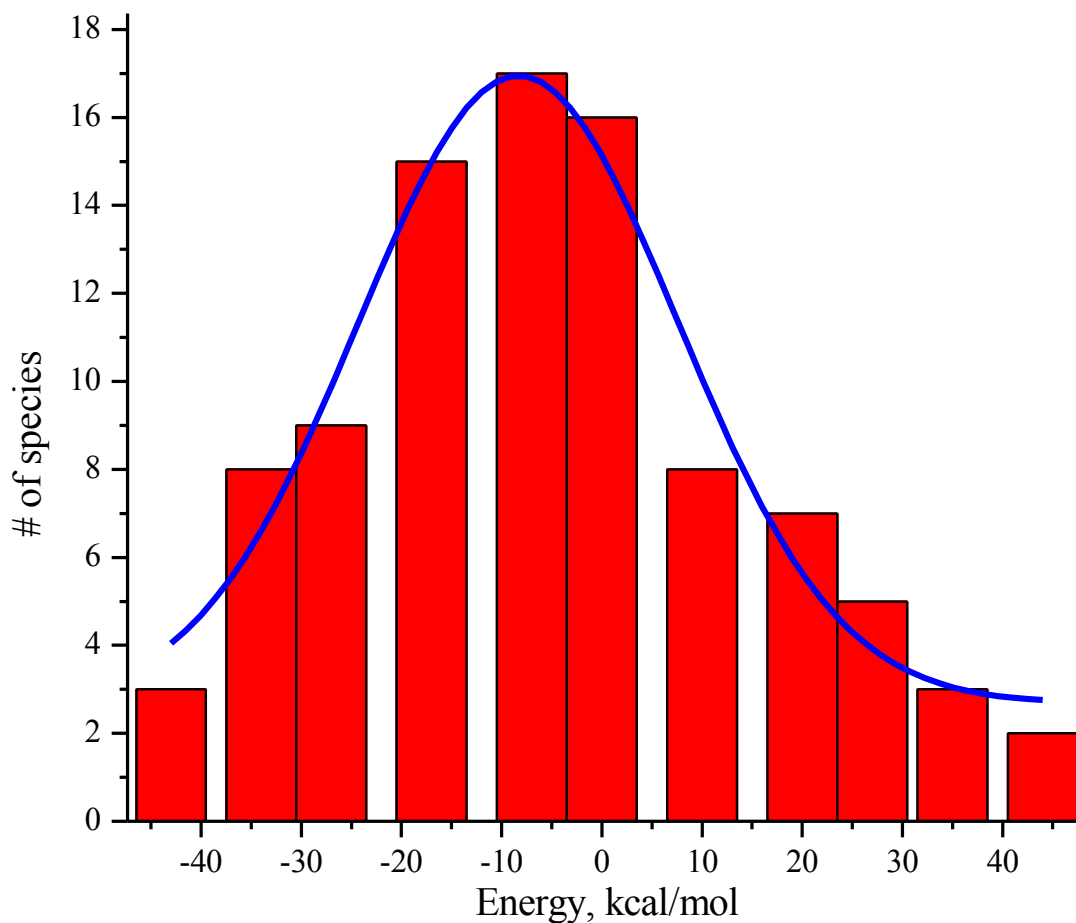
Figure S2.6. A distribution of the QM/MM-generated phase initial condition (red bars) and exponential fit, represented as number of species vs. its relative energy.

It is clearly seen that the initial conditions distribution, generated for QM/MM molecular dynamics slightly deviates from the Gaussian (c.a. gas-phase). It is due to the algorithm I used to generate the gas-phase initial condition forces them to be Gaussian whereas in QM/MM case it if nearly random. To get the perfect Gaussian distribution one may need to generate not one hundred, but a few thousand points.

CHAPTER 3: DIRECT PHOTOISOMERIZATION OF CH_2I_2 VS $CHBR_3$ IN THE GAS

PHASE: A JOINT 50 FS EXPERIMENTAL AND MULTIREFERENCE RESONANCE-

THEORETICAL STUDY

Abstract

Femtosecond transient absorption measurements powered by 40 fs laser pulses reveal that ultrafast isomerization takes place upon S_1 excitation of both CH_2I_2 and $CHBr_3$ in the gas phase. The photochemical conversion process is direct and intramolecular, i.e., it proceeds without caging media that have long been implicated in the photo-induced isomerization of polyhalogenated alkanes. Using complete active space second order perturbation theory (CASPT2) calculations, we investigate the structure of the photochemical reaction paths connecting the photoexcited species to their corresponding isomeric forms. Unconstrained minimum energy paths computed starting from the S_1 FC points lead to S_1/S_0 conical intersections, which connect the parent $CHBr_3$ and CH_2I_2 molecules to their isomeric forms, and after the intersections directly to the isomeric forms without the intermediacy of primary photodissociation products. The changes in the chemical bonding along the S_1/S_0 isomerization reaction path are described using multireference average coupled pair functional (MRACPF) calculations in conjunction with the natural resonance theory (NRT) analysis. These calculations reveal a complex interplay between covalent, radical, ylidic, and ion-pair dominant resonance structures throughout the photochemical isomerization paths described in this work.

Introduction

The UV photodissociation reactions of naturally occurring and man-made di- and polyhalogenated alkanes are ubiquitous sources of reactive halogens that have impact on atmospheric and environmental chemistry.[1-4] Much work in the area of gas-phase reaction dynamics has been devoted to elucidating the elementary steps involved at atomic/molecular level in the photodissociation process.[5-8] Polyatomic radical and halogen atom fragments have been detected,[9-16] and the low-energy excited-states of di- and polyhalogenated alkanes were found to be repulsive with respect to an increase in the carbon-halogen bond lengths in the Franck-Condon (FC) region.[17,18] As a result, it has long been assumed that excitation of these molecules exclusively results in direct photodissociation,[19-38] that is the smooth separation of polyatomic radical and halogen atom fragments out to the asymptotic limit without trapping in an intermediate state. However, photochemical studies in solution and condensed phase identified other major reaction product of di- and polyhalogenated alkanes, namely, the *iso*-halocarbon species featuring C–X–Y bonding motifs (X, Y = Cl, Br, and I).[28,31,32,39-42] In this context, isomer formation has long been associated with a cage-induced isomerization mechanism, whereby collisions with the surrounding solvent molecules arrest the separating halogen atom and polyatomic radical primary products, and cause them to recombine to form an *iso*-halocarbon.[28,31-38,40-44] Recent ultrafast transient absorption experiments probing the photochemistry of $CHBr_3$, BBr_3, and PBr_3 in solution revealed that their corresponding *iso*-halocarbon photoproducts are formed within 100 fs following S_0-S_1 excitation.[45,46] This was a significant finding; the photoisomerization occurred faster than solvent caging times, even if the caging were due to a single collision.[46] Even more surprisingly, the BrHCBr–Br isomer was observed on the same time scale following UV irradiation of $CHBr_3$ *in the gas phase*.[46] Quantum

chemical simulations of $CHBr_3$, BBr_3, and PBr_3 showed that following S_0-S_1 excitation of these geminal tribromides, what initially appears to be simple fission of a bond between the central atom and one of the bromines is in fact direct isomerization that occurs through the roaming of molecular fragments on the flat regions of the S_1 and S_0 potential energy surfaces.[46] Throughout the isomerization process, which the simulations suggest takes place on a 50-fs time scale, the excited parent molecule 'roams' into the ground-state well of the isomer through a conical intersection.[46] To date, the latter study was the first and only demonstration of the direct formation of *iso*-halocarbons from photoexcited halogenated alkanes. The present study builds on and expands the scope of the prior work. We first report the photoisomerization dynamics of $CHBr_3$ and CH_2I_2 in the gas-phase following S_0-S_1 excitation of these two molecules at 250 and 330 nm, respectively. In contrast with the attainable laser pulses in the prior work (90 fs), our current transient absorption measurements are powered by 40 fs laser pulses in the deep UV and UV range, the generation of which with the energy sufficient to excite poor absorbers such as small polyatomic molecules is non-trivial.[47,48] Pulses with temporal duration below 50 fs are essential for both (i) resolving nuclear motions in halogenated alkanes, featuring time periods in the 30 to 100 fs range, and (ii) following photochemical reaction dynamics previously predicted to occur on a ~50 fs time scale.[46] Second, we complement our experimental work with non-standard quantum chemical simulations, which trace the evolution from a familiar bonding situation in the photoexcited parent molecules to a non-conventional bonding motif in the ground-state isomer photoproducts, and which is of direct relevance to photochemistry and photochemical applications of these molecules.

Ground-state isomers of haloalkanes occupy shallow minima of several kcal mol^{-1} from a radical dissociation pathway,[22,32,46,49-52] i.e., the energy required to break a carbon-halogen bond

in the parent halocarbon. The chemical bonding picture in such highly energetic and unusual species has been of considerable interest.[28,39,40,44,53-56] Prior works suggested a predominantly contact ion pair resonance structure for *iso*-halocarbons.[28,36,39,40,44,53-55,57-61] Understanding the manner in which chemical bonding changes and net charge becomes redistributed along the photochemical isomerization path may provide novel pathways towards controlling chemical reactivity. Yet, assessing this understanding poses a significant challenge from a theoretical viewpoint, since the method of choice ought to describe the complex electronic character of the non-adiabatic photochemical transformation at hand. The conventional methods used this far to describe the *iso*-halocarbons, including tools of density functional theory (DFT) and second order Möller–Plesset perturbation theory (MP2), do not properly describe regions of the potential energy surface (even on S_0) in the vicinity of electronic degeneracy.[62] With the above considerations in mind, we will employ tools of multi-reference quantum chemistry to describe both the photochemical reaction path connecting the S_1 CHBr$_3$ and S_1 CH$_2$I$_2$ to their isomeric S_0 forms as well as the change in the nature of chemical bonding throughout the photochemical conversion process.

Our molecular dynamics and transient absorption results suggests that BrHCBr–Br decays into CHBr$_2$ and Br.[46] We suggest that the decay of *iso*-CH$_2$I$_2$ produces CH$_2$I and ground-state I($^2P_{3/2}$), following previous photofragment spectroscopy and imaging experiments,[11,15,16] where CH$_2$I and I($^2P_{3/2}$) are the sole photoproducts observed following S_1-excitation of CH$_2$I$_2$. On the basis of our observations, we conclude that dissociation does take place, but rather, it is a result of the further dissociation of the primary *iso*-halogen photoproducts. The dissociation is thus neither direct nor takes place on a sub-100 fs time scale, at least for a substantial fraction of photoexcited CHBr$_3$ and CH$_2$I$_2$ molecules. At this stage, whether all the photodissociation

products are formed through the aforementioned mechanism is unclear; the possibility of two parallel processes, one of which is direct dissociation cannot be excluded on the basis of our observation. To the best of our knowledge, the isomeric species were never observed in previous photofragment translational spectroscopy and ion imaging studies of halogenated alkanes, even upon excitation into low-lying (< 5 eV) electronic states, although such anomalies as fragment broad translational energy distribution and partial loss of anisotropy were reported for CH_2I_2[12,15,16] and CH_2Cl_2.[70] Since the isomer lifetime is short (somewhat less than 150 fs), one may wonder if the isomerization channel may be reliably detected through fragment anisotropy and translational energy. In contrast, herein we demonstrate that 40-fs transient absorption allows detecting this key reaction intermediate.

Modern computational methods make it possible to trace the evolution of molecular and electronic structure from the Franck-Condon point to the photoproducts on the ground electronic state *via* the pathway of least resistance,[63] much like connecting the reactant and product species *via* a transition state along the thermal reaction pathway.[64] The resulting photochemical minimum energy path (MEP) characterizes the most favorable relaxation pathway. The MEP for both $CHBr_3$ and CH_2I_2, computed by means of Complete Active Space Perturbation Theory (CASPT2) - one of the most accurate methods for excited-state studies (accuracy < 6.9 kcal mol^{-1}),[65,66] suggest that the S_1 gradient at the FC point steers the molecule on a steep downhill barrierless path, Figures 2 and 3. The initial motion out of the FC region proceed predominantly via a significant elongation of a carbon-halogen bond coupled to the umbrella and CBr_2/CI_2 scissor motions, consistent with previous resonance Raman investigations.[17,30,67,68] Towards the end of the steep part of the S_1 MEP the degree of the elongation of the C–Br and C–I bonds decreases. As the S_1 potential flattens out, it reaches a CI

between the S_1 and S_0 states. In the CI region, the stretched C–Br and C–I bonds are partially dissociated. At the same time, it appears that the dissociating halogen atom interacts with the halogen bound to the polyatomic fragment. Indeed, although the corresponding halogen-halogen distances (4.24 Å in $CHBr_3$ and 4.20 Å in CH_2I_2, Table 3.5S,3.6S in Supporting Information) are somewhat larger the sum of van der Waals radii for symmetrical halogen interaction (Br$\cdots$Br 3.70 Å and I$\cdots$I 3.96 Å) and close to upper limits at which halogen atoms are still interacting (~4 Å),[54,69,70] the opposite partial charges on the involved halogens (see below) ensure their reasonable attractive interaction. Calculations of the MEP after the S_1/S_0 CI yields a gently-sloped ground-state potential, which is associated with the opening of the C–Br–Br and C–I–I angles, the planarization of $CHBr_2$ and CH_2I fragments to a significant degree and the development of the Br–Br and I–I bonds. The MEP eventually reaches a ground-state minimum corresponding to the isomers, *iso*-$CHBr_3$ and *iso*-CH_2I_2. The stationary points corresponding to isomer minima were previously computed in several studies for several halocarbons,[22,49-52,71] but our present work on CH_2I_2 and $CHBr_3$ uniquely demonstrates that the FC region, where the photoreaction begins, is indeed connected to the isomer minimum *via* an exothermic barrierless route mediated by an S_1-S_0 conical intersection.
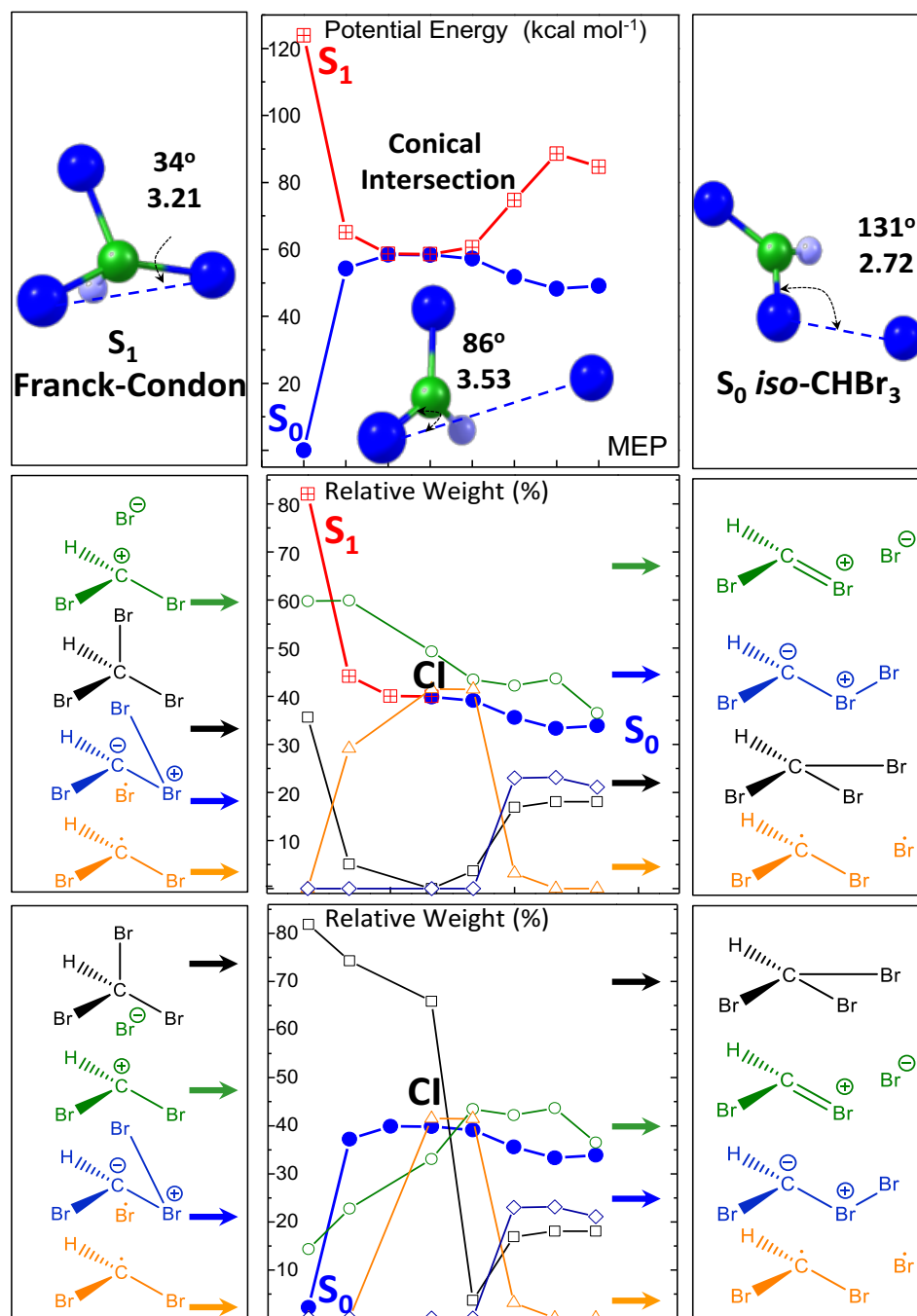
Figure 3.1. CHBr$_3$. Top panel: the MEP initiated at the S$_1$ Franck-Condon (FC) point and, after the S$_1$/S$_0$ conical intersection (CI), resumed on the S$_0$ state. The structures of the FC point, CI, and isomer are shown in the inset. Middle panel: Major resonance forms along the photochemical MEP and their relative weights. Bottom panel: the contribution of major resonance forms along the ground-state path connecting two isomeric forms. In the later, the energy profile from the CI to the parent, which is obtained as single-point energy computations from the S$_1$ MEP, practically coincides with the ground-state MEP computed from the CI to the parent.

Not surprisingly, previously computed low-lying excited electronic states of CH_2I_2 computed along a single co-ordinate (e.g., the C−I bond length) were found to be repulsive,[23,43,72] supporting the commonly adopted premise that the sole *primary* photochemical products are the CH_2I and I fragments.[11-43] Herein, we find that the picture painted by the previous works based on scanning a single coordinate at a time, see also studies on other structurally related halogenated alkanes,[73-77] naturally misses out on the multidimensional character of the photochemical transformation described herein using the more chemically relevant MEP methodology. Furthermore, the computed CIs are situated at much lower energy than the FC point, and therefore, are energetically accessible 'funnels' for non-adiabatic relaxation of the excited parent molecules. Isomerization of S_1 $CHBr_3$ mediated by the conical intersection is also supported by molecular dynamics simulations.[46] This CI is very close in terms of molecular structure to the one computed in Figure 3.1. The formation of the BrHCBr–Br isomer product on a sub-100 fs time scale without the need of a caging medium is uniquely illustrated in our above-described transient absorption experiments. The MEP of CH_2I_2 shows topological features similar to that of $CHBr_3$, Figures 2 and 3. Therefore, direct isomerization is also expected to occur for S_1 CH_2I_2, in agreement with the experimental data.

Weinhold, Weiss and co-workers were the first who suggested that the transient intermediate formed upon irradiation of liquid haloalkane (CCl_4) is its isomer and proposed that isomers may play an important role in the chemistry of heavier halides.[39] Their computational study constitutes the first effort to understand the chemical bonding in *iso*-species. Natural bond orbital (NBO) analysis suggested the contact ion pair nature of *iso*-CCl_4, $Cl_2C-Cl^{+\cdots}Cl^-$.[39] The authors also noted that the donor stabilized geminal diiodo-compounds are likely to be described as a three-center four-electron hypervalent species, the prediction later confirmed by their nearly

linear C−I−I structures revealed by X-ray data.[78,79] On the basis of matrix-isolation IR spectra and computed charges, Maier, Reisenauer, and co-workers concluded that the hypervalent ($H_2C=X−Y$) and two contact ion pair forms ($H_2C^+−X \cdots Y^-$ and $H_2C=X^{+} \cdots Y^-$) contribute primarily to the *iso*-dihalomethanes structure.[28,40] Forms such as a halonium ylide $H_2C^-−X^+−Y$, a carbene-dihalogen $H_2C \cdots XY$ complex, an open-shell $H_2C \cdot −X \cdot −Y$ singlet, and a $H_2C \cdot −X \cdots Y \cdot$ radical pair were considered to be unimportant. Neither the charge distribution nor the bent C−I−I structure
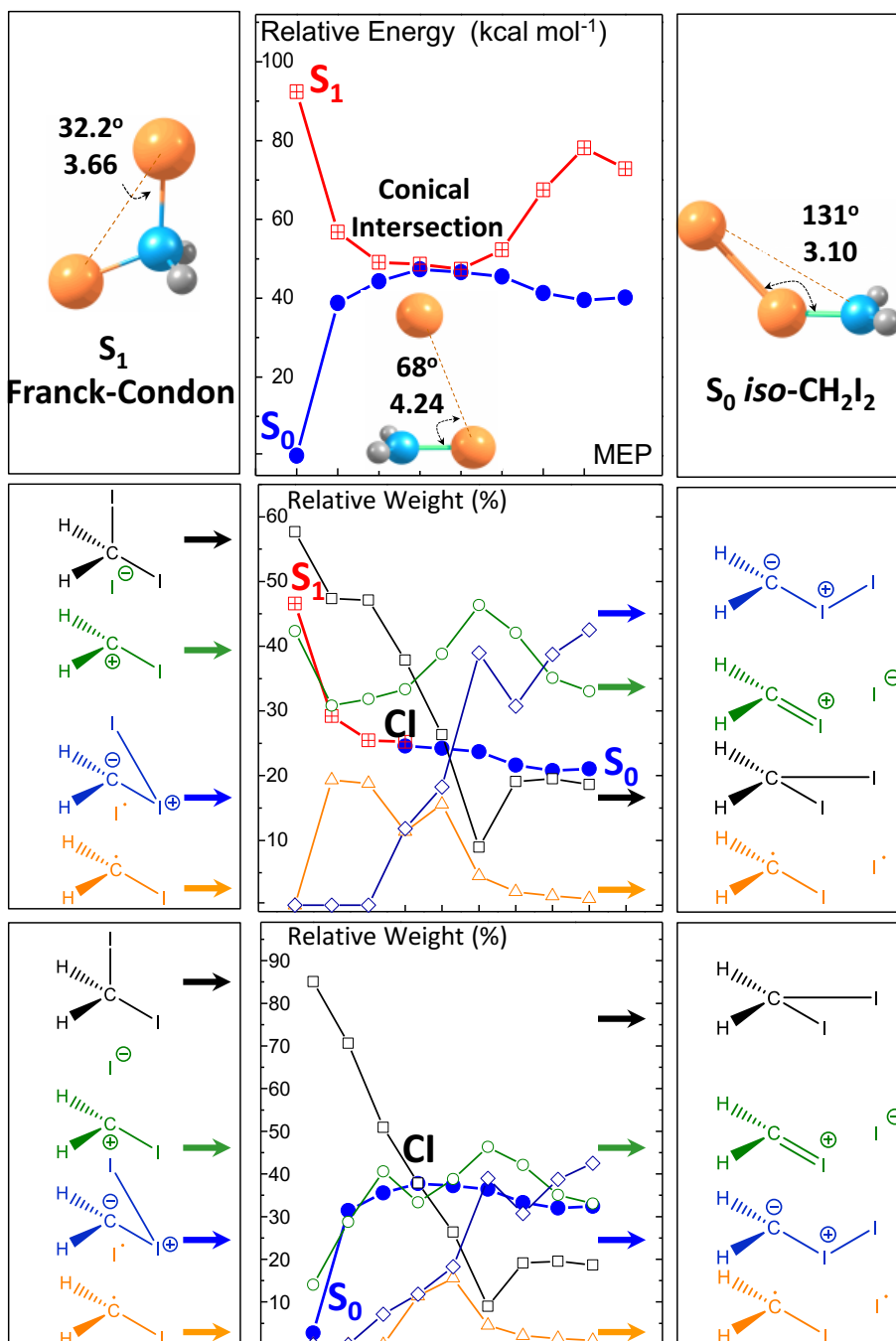
Figure 3.2. The CH_2I_2 S_1/S_0 MEP. The Franck-Condon, conical intersection, and isomer structures (top panel), major resonance forms and their relative weight along this photochemical MEP (middle panel) and along the ground-state path connecting two isomers (bottom panel) are all illustrated in this plot. For more details, the reader is referred to Figure 2 captions.

computed for *iso*-CH$_2$I$_2$ agreed with the hypervalent description of this species.[54] The structurally related *iso*-CH$_2$Cl$_2$ was described as a resonance hybrid of a chloromethyl cation plus a chloride ion and a halohium ylide.[55] With the original suggestion by Weinhold and Weiss overlooked, the formation of isomer photoproducts in room-temperature liquid solutions containing halocarbons were not suspected until the ultrafast transient absorption study of CH$_2$I$_2$.[31] Subsequent solution studies indicated that the relative contribution of ion-pair forms increases with solvent polarity, as expected.[36,57] Finally, Reid and co-workers computed the ground-state MEP connecting the transition state with the parent and *iso*- species for several halocarbons (CHBr$_3$, CFBr$_3$, CH$_2$Br$_2$, and CCl$_4$[44,59-61]) using MP2 and DFT methods and applied Natural Resonance Theory (NRT) to compute weighs of resonance structures along the reaction path. The authors concluded that the isomers are described by ion-pair resonance forms with much smaller covalent and ylide contributions and that the ground-state isomerization is a crossover from the covalent-dominated structure of the parent to the ion-pair dominated structure of the isomer.

In the present work, we describe the contribution of resonance forms along the photoisomerization path by means (NRT),[80-82] which now can be applied to describe and
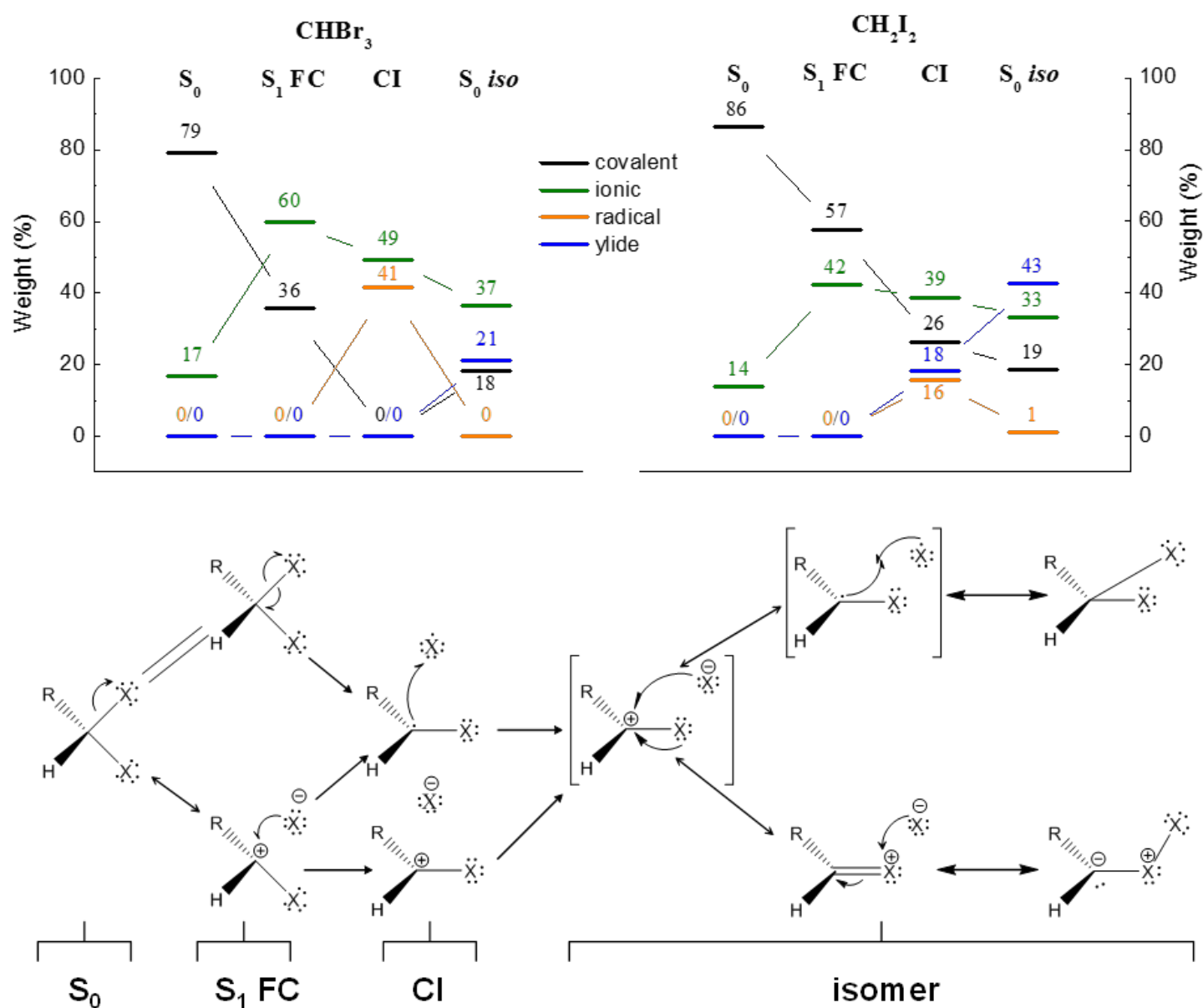
Figure 3.3. Top panel: numeric contributions (weights, %) of different resonance forms shown at key points (parent S_0 and S_1, CI, isomer) along the photochemical MEP for bromoform (left) and diiodomethane (right). Bottom panel: generic electron 'arrow pushing' scheme for CH_2I_2 and $CHBr_3$ that connects various resonance structures encountered along the photochemical MEP. Resonance forms with contributions of less than 5% are shown in square parentheses.

excited states and state crossing regions,[83] in conjunction with Multireference Averaged Coupled Pair Functional (MRACPF)[84]. Unlike prior works, our calculations account for the complex character of the wavefunctions evolving from the FC region on the excited electronic state to the ground state well through a conical intersection. We found that in the case of $CHBr_3$ and CH_2I_2, four resonance forms – a contact ion pair between a halide and a halocarbenium with the negative charge on the halogen, a covalent structure, a halonium ylide, and a radical pair - primarily contribute to the electronic structures encountered along the photochemical MEP. Excitation into S_1 changes the electronic structure of ground-state $CHBr_3$ from 82% covalent (the second-largest weight is that of the ion-pair, ~14%) to predominantly ionic (60%) with other ~40% remaining covalent, Figure 2. The ion pair weight reaches the maximum at the FC point, but gradually decreases along the MEP. Still, there is a significant presence of this form in the CI region (49%) and towards the isomer minimum (37%). It can be seen that along the path from the FC to the CI point, the covalent weight decreases from ~40 to ~0%, whereas the radical pair weight increases by a comparable amount. As a result, the radical and ion-pair structures have nearly the same weight in the CI region. On the S_0 surface from the CI point to the *iso*-$CHBr_3$ minimum, the contributions of the covalent and ylide structures grow by comparable amounts to ~20% at the expense of the radical pair form, the contribution of which sharply decreases from 41% to 0. The equilibrium structure of *iso*-$CHBr_3$ is 37% ion-pair with nearly the same total contribution from the covalent and ylidic resonance forms. Along the S_0 path from the CI, which is close in terms of molecular structure to the isomerization transition state that links $CHBr_3$ and *iso*-$CHBr_3$,[45] in the direction of $CHBr_3$, the weight of the radical and ion-pair forms decreases whereas that of the covalent form increases. In CH_2I_2, the optimized parent structure is 86% covalent and 14% ionic. The electronic structure of the S_1 FC point is 57% covalent and 42%

ion-pair, Figure 3. Along the S_1 MEP towards the CI, the weight of the covalent and ion-pain structures decreases whereas that of the radical structure increases by about the same amount. At the CI, the ylide form modestly contributes

to the overall bonding pictures. The electronic structure on the S_0 MEP from the CI towards *iso*-CH_2I_2 becomes progressively more ylide- and ion-pair-like at the cost of the radical and covalent forms. The *iso*-CH_2I_2 equilibrium structure is mostly ylidic (43%) with a large contribution of the ion-pair (33%) and a much smaller contribution of the covalent form (19%). Thus, the overall picture for these two halocarbons is that following excitation, the electronic structure 'hesitates' between being covalent or ionic, Figure 4. The radical structure originates from the covalent structure at the CI as a result of decoupling of the electrons on the C−X σ-bond. On the isomer side of the S_0 potential, the radical form fades away as a result of: (i) the reformation of the covalent form via remaking of the σ-bond; (ii) formation of the ylide form with the negative charge localized on the carbon and the positive charge on the inner halogen. The radical pair form was not detected in previous DFT and MP2 investigations.[44,59-61] We attribute the latter to limitations of the aforementioned single-configurational methods that cannot accurately describe homolytical bond breaking processes. Detailed insights require the investigation of the homological series, but one can note that the presence of less electronegative dihalogen next to the carbon (I−I *vs.* Br−Br) seems to stabilize the negative charge on the carbon, i.e. favoring the ylide. Finally, although photoelimination of molecular halogen was suggested for $CHBr_3$ and CH_2I_2 on excitation with low-energy UV photons,[22,52,85-87] albeit in a small quantum yield for the latter molecule, the resonance form representing a carbene-dihalogen complex possibly involved does not carry any significant weight (> 5%) along both MEPs.

Conclusion

We demonstrate the occurrence of direct isomerization of S_1-excited CH_2I_2 and $CHBr_3$ in the gas phase. The isomerization occurs via internal rearrangement of the parent halocarbon molecule and leads to the formation of short-lived (~100-150 fs) ground-state isomers with an I−I and a Br−Br bond. The isomerization process is seen in transient absorption signals spread over the first 200 fs after photoexcitation. The time resolution of the experiments (~30 fs), which is on a time scale of skeletal motion in halocarbons, allows direct time-resolved observation of this unusual isomerization dynamics and the population of the isomer trapping site. Our results show that for a substantial fraction of S_1 $CHBr_3$ and S_1 CH_2I_2 the photodissociation is neither direct nor takes place on a sub-100 fs time scale, but happens, quite unexpectedly, from the electronic ground state of the isomer primary product. The formation of the isomeric species, known to be reactive,[34,36,37,44] under atmospheric conditions may have an influence over the kinetics of the associated reactions by affecting the energy partitioning of the reaction products and lead to unexpected reaction channels, also in the presence of a stabilizing environment capable of relaxing excess vibrational energy such as airborne particles.

Direct isomerization is consistent with the minimum energy path (MEP) computed using CASPT2 from the Franck-Condon S_1 point of $CHBr_3$ and CH_2I_2. The MEPs show that other nuclear motions, in addition to carbon-halogen stretching, primarily an opening of a C–I–I-and a C–Br–Br angle, contribute to the reaction coordinate. The S_1 PESs are barrierless and exothermic, and show conical intersections situated at much lower energy than the Franck-Condon point, and therefore, energetically accessible. After the CIs, the MEPs on the S_0 surface directly lead to the isomer species, *iso*-$CHBr_3$ and *iso*-CH_2I_2, rather than to radical pairs. The

presence of the CIs known to be responsible for extremely rapid radiationless relaxation in molecules is consistent with the ultrafast isomerization observed.

Our work provides the first evidence of direct photoisomerization for CH_2I_2. Previous works in which (i) resonance Raman studies showed that the dissociation of S_1 CH_2I_2 is direct in the sense that the wavepacket does not revisit the FC region, (ii) computational studies showing that low-lying excited states of CH_2I_2 along a C−I bond length are repulsive, and (iii) photofragment translational spectroscopy and ion imaging detection of CH_2I and I fragments seemingly yield a self-consistent picture of the CH_2I_2 photodissociation. However, transient absorption experiments with sub-40 fs temporal resolution complemented by tools of multireference quantum chemistry herein show that this is not the case for a substantial fraction of S_1 population.

Electronic structure calculations along the 'photochemical' MEPs were also performed using the MRACPF methodology in conjunction with the NRT analysis. To the best of our knowledge, our work provides the first *quantitative* reliable description of the photochemical reaction path, including the CI region, in terms of the contributing resonance forms. On S_0, MRACPF overcomes the shortcomings of single-reference methods in describing structures in situations where electronic degeneracy is encountered. The NRT analysis performed on the MRACPF wavefunction to obtain major contributing resonance forms into the electronic structure suggests that the ion-pair form is dominant in the FC region and remains significant along the entire MEP, including the ground-state isomer well. Ylide and covalent forms also contribute significantly to the overall electronic structure of the isomer species, whereas the radical pair form is significant through the conical intersection region, both on S_1 and S_0. A correct description of the resonance structures encountered is the key to rationalizing the ways in

which chemical bonding changes and net charge redistributes in a photochemical reaction in general, and may open new ways to control chemical reactivity. The examination of the solvent ability to steer the photochemical transformations towards a desired path is a possible extension, and further work is warranted in this regard. Overall, the general approaches and methodologies described herein should be transferrable and applicable to a wealth of photochemical transformations involving small and moderately-sized molecules.

Methodology

In computational studies, the steepest-descent MEP computations in mass-weighted Cartesian coordinates are carried out using multistate (MS) CASPT2 method with 6-311G** basis set, Molcas 7.8 program package.[89] $CHBr_3$ and CH_2I_2 were optimized on the ground electronic state (S_0). The active space was chosen to consist of 12 electrons in 9 orbitals (three state averaging), which closely reproduces the energy of the first singlet excited state (S_1) in $CHBr_3$ (5.36 *vs*. 5.10 eV[64]) and CH_2I_2 (4.10 *vs*. 3.97-4.02 eV[11]). For both $CHBr_3$ and CH_2I_2, the MEP step was 0.4 Bohr. The MEPs were initiated from the FC point on the S_1 potential end in the region where the energy difference between the S_1 and S_0 states becomes less than 2 kcal/mol, which suggests a conical intersection (CI) between the S_1 and S_0 surfaces.[90] The investigation of the geometrical phase effect confirms the presence of the S_1/S_0 CI in both systems, see Supporting Information. After the CI, the MEPs resumed on the S_0 surface reach the equilibrium structure of the corresponding *iso*-species. For each geometry point on the MEPs, the ground- and excited-state wavefunctions and density matrices were generated using MRACPF/6-311G** method, as implemented in Orca 3.0.3 program.[91] The reference space for MRACPF is based on the CASSCF wavefunction (14 electrons in 10 orbitals) with automatic selection of reference configurations (threshold, 10^{-4}). NRT analysis, as implemented in NBO 6.0

program package,[92] is based on the input generated via Orca-NBO interface. The weight of a resonance structure is the probability with which the structure enters the total density matrix. All resonance structures, apart from four dominant ones, were found to contribute less than 5% each, see Supporting Information.

References

[1] Barrie, L. A.; Bottenheim, J. W.; Schnell, R. C.; Crutzen, P. J.; Rasmussen, R. A. *Nature* **1988**, *334*, 138-141.

[2] O'Dowd, C. D.; Jimenez, J. L.; Bahreini, R.; Flagan, R. C.; Seinfeld, J. H.; Hämeri, K.; Pirjola, L.; Kulmala, M.; Jennings, S. G.; Hoffmann, T. *Nature* **2002**, *417*, 632-636.

[3] Carpenter, L. *Chem. Rev.* **2003**, *103*, 4953-4962.

[4] Quack B.; Wallace, D. W. R. *Global Biogeochem. Cycles* **2003**, *17*, 1023, doi:10.1029/2002GB001890, 1.

[5] Butler, L. J.; Neumark, D. M. *J. Phys. Chem.* **1996**, *100*, 12801-12816.

[6] Sato, H. *Chem. Rev.* **2001**, *101*, 2687-2725.

[7] Zewail, A. H. *J. Phys. Chem.* **2000**, *104*, 5660-5694.

[8] Hertel, I. V.; Radloff, W. *Rep. Progr. Phys.* **2006**, *69*, 1897-2003.

[9] Gregory, R. A.; Style, D. W. G. *Trans. Faraday Soc.* **1936**, *32*, 724-736.

[10] Gibson, K. E.; Iredale, T. *Trans. Faraday Soc.*, **1936**, *32*, 571-576.

[11] Kawasaki, M.; Lee, S. J.; Bersohn, R. *J. Chem. Phys.* **1975**, *65*, 809-814.

[12] Kroger, P. M.; Demou, P. C.; Riley, S. J. *J. Chem. Phys.* **1976**, *65*, 1823-1834.

[13] Schmitt, G.; Gomes, F. J. *J. Photochem.* **1980**, 14, 107-123.

[14] Baughcum, S. L.; Leone, S. R. *J. Chem. Phys.* **1980**, *72*, 6531-6545.

[15] Jung, K.-W.; Ahmadi, T. S. El-Sayed, M. A. *Bull. Korean Chem. Soc.* **1997**, *18*, 1274-1280

[16] Xu, H.; Guo, Y.; Liu, S.; Ma, X.; Dai, D.; Sha, G. *J. Chem. Phys.* **2002**, *117*, 5722-5729.

[17] Zhang, J.; Imre, D. G. *J. Chem. Phys.* **1988**, *89*, 309-313.

[18] Zhang, J.; Heller, E. J.; Huber, D.; Imre, D. G. *J. Chem. Phys.* **1988**, *89*, 3602-3611.

[19] Miranda, M. A.; Pérez-Prieto, J.; Font-Sanchis, E.; Scaiano, J. C. *Acc. Chem. Res.* **2001**, *34*, 717-726.

[20] Jones, C.E.; Carpenter, L. J. *Environ. Sci Tech.* **2005**, *39*, 6130-6137

[21] Lehman, J. H.; Li, H. W.; Lester, M. I. *Chem. Phys. Lett.* **2013**, *590*, 16-21.

[22] Chen, S.-Y.; Tsai, P.-Y.; Lin, H.-C.; Wu, C.-C.; Lin, K. C.; Sun, B. J.; Chang, A. H. H. *J. Chem. Phys.* **2011**, *134*, 034315.

[23] Mandal, A.; Singh, P. J.; Shastri, A.; Jagatap, B. N. *J. Chem. Phys.* **2014**, *140*, 194312.

[24] Barinovs, G.; Markovic, Nyman G. *J. Chem. Phys.* **1999**, *111*, 6705-6711.

[25] Kropp, P. J.; Poindexter, G. S.; Pienta, N. J.; Hamilton, D. C. *J. Am. Chem. Soc.* **1976**, *98*, 8135-8144.

[26] Pienta, N. J.; Kropp, P. J. *J. Am. Chem. Soc.* **1978**, *100*, 655-657.

[27] Pienta, N. J.; Kropp, P. J. *Acc. Chem. Res.* **1984**, *17*, 137-144.

[28] Maier, G.; Reisenauer, H. P. J. Hu, Schaad, L. J.; Hess, B. A. Jr. *J. Am. Chem. Soc.* **1990**, *112*, 5117-5122.

[29] Schwartz, B. J.; King, J.; Zhang, J. Z.; Harris, C. B. *Chem. Phys. Lett.* **1993**, *203*, 503-508.

[30] Kwok, W. M.; Phillips, D. L. *J. Chem. Phys.* **1996**, *104*, 2529-2540.

[31] Tarnovsky, A. N.; Alvarez, J.-L.; Yartsev, A. P.; Sundström, V.; Åkesson E. *Chem. Phys. Lett.* **1999**, *312*, 121-130.

[32] Zheng, X.; Phillips, D. L. *J. Phys. Chem. A* **2000**, *104*, 6880-6886.

[33] Kwok; W. M.; Ma C. S.; Parker, A. W.; Phillips, D.; Towrie, M.; Matousek, P.; Phillips, D. L. *J. Chem. Phys.* **2000**, *113*, 7471-7478.

[34] Phillips, D. L.; Fang, W.-H.; Zheng, X. *J. Am. Chem. Soc*. **2001**, *123*, 4197-4203.

[35] Wall, M.; Tarnovsky, A. N.; Pascher, T.; Sundström, V.; Åkesson, E. *J. Phys. Chem. A* **2003**, *107*, 211-217.

[36] Tarnovsky, A. N.; Sundström, V.; Åkesson, E.; Pascher, T. *J. Phys. Chem. A* **2004**, *108*, 237-249. Additions/corrections: *ibid*. **2005**, *109*, 954–954.

[37] Phillips, D. L.; Fang, W.-H.; Zheng, X.; Li, Y.-L.; Wang, D.; Kwok, W. M. *Curr. Org. Chem.* **2004**, *8*, 739-755.

[38] Crim, F. F. *Faraday Disc.* **2012**, *157*, 9-26.

[39] Reed, A. E.; Weinhold, F.; Weiss, R. Macheleid, J. *J. Phys. Chem.* **1985**, *89*, 2688-2694.

[40] Maier, G.; Reisenauer, H. P. *Angew. Chem. Int. Ed. Engl.* **1986**, *25,* 819-822.

[41] Davidsson, J.; Poulsen, J.; Cammarata, M.; Georgiou, P.; Wouts, R.; Katona, G.; Jacobson, F.; Plech, A.; Wulff, M.; Nyman, G.; Neutze, R. *Phys. Rev. Lett.* **2005**, *94*, 245503.

[42] Vincent, J.; Andersson, M.; Eklund, M.; Wöhri, A. B.; Odelius, M.; Malmerberg, E.; Kong, Q.; Wulff, M.; Neutze, R.; Davidsson, J. *J. Chem. Phys.* **2009**, *130*, 154502.

[43] Odelius, M.; Kadi, M.; Davidsson, J.; Tarnovsky, A. N. *J. Chem. Phys*. **2004**, *121,* 2208-2214.

[44] Reid, S. A. *Int. Rev. Phys. Chem.* **2014**, *33*, 341-370.

[45] Pal, S. K.; Mereshchenko, A. S.; Butaeva, E. V.; El-Khoury, P. Z.; Tarnovsky, A. N. *J. Chem. Phys.* **2013**, *138*, 124501/1-19.

[46] Mereshchenko, A. S.; Butaeva, E. V.; Borin, V. A.; Eyzips, A.; Tarnovsky, A. N. *Nature Chem.* **2015**, *7*, 562-568.

[47] Jailaubekov, A. E.; Bradforth, S. E. *Appl. Phys. Lett.* **2005**, 87, 021107-1-3.

[48] Homann, C.; Lang, P.; Riedle, E. *J. Opt. Soc. Am. B* **2012**, *29* 2765-2769.

[49] Tweeten, E. D.; Petro, B. J.; Quandt, R. W. *J. Phys. Chem. A* **2003**, *107*, 19-24.

[50] McDonald, K. J.; Quandt, R. W. *Comput. Theor. Chem.* **2014**, *1037*, 28-34.

[51] Kalume, A.; George, L.; Reid, S. A. *J. Phys. Chem. Lett.* **2010**, *1*, 3090-3095.

[52] Lin, K.-C.; Tsai, P.-Y. *Phys. Chem. Chem. Phys.* **2014**, *16*, 7184-7198.

[53] Weiss, R. Rechinger, M. Hampel, F. *Angew. Chem. Int. Ed. Engl.* **1994**, *33,* 893-895.

[54] Bach, R. D.: Glukhovtsev, M. N. *Chem. Phys. Lett.* **1997**, *269*, 145-150.

[55] Lewars, E. *J. Mol. Str. Theochem.* **1998**, *425*, 207-226.

[56] Orel, A. E.; Kühn O. *Chem. Phys. Lett.* **1999**, *304*, 285–292.

[57] El-Khoury. P. Z.; Pal, S. K.; Mereshchenko, A. S.; Tarnovsky, A. N. *Chem. Phys. Lett.* **2010**, *493*, 61-66.

[58] El-Khoury, P. Z.; George, L.; Kalume, A.; Reid, S. A.; Ault, B. S.; Tarnovsky, A. N. *J. Chem. Phys.* **2010***, 132*, 124501/1-11.

[59] George, L.; Kalume, A.; Esselman, B. J.; Wagner, J.; McMahon, R. J; Reid, S. *J. Chem. Phys*. **2011**, *135*, 124503/1-8.

[60] George, L.; Kalume, A.; Reid, S. A.; J. Esselman, B.; McMahon, R. J. *J. Mol. Str.* **2012**, *1025*, 61-68.

[61] Abou-Chaline, F.; Preston, T. J.; Dunning, G. T.; Orr-Ewing, A. J.; Greetham, G. M.; Clark, I. P.; Towrie, M.; Reid, S. A. *J. Phys. Chem. A* **2013**, *117*, 13388-13398.

[62] Levine, B. G.; Ko. C.; Quenneville, J.; Martinez, T. J. *Mol. Phys.* **2006**, *104*, 1039-1051.

[63] Bernardi, F.; Olivucci, M.; Robb, M.A. *Chem. Soc. Rev.* **1996**, *25*, 321-328.

[64] Marom, R.; Golan, A.; Rosenwaks, S.; Bar, I. *J. Phys. Chem. A* **2004**, *108*, 8089-8095.

[65] Hratchian, H. P.; Schlegel, H. B. Finding Minima, Transition States, and Following Reaction Pathways on *Ab Initio* Potential Energy Surfaces. *Theory and Application of Computational Chemistry: The First Forty Years*, Elsevier B.V., **2005**; p. 195-249.

[66] Pulay, P. A. *Int. J. Quant. Chem.* **2011**, *111*, 3273-3279.

[67] Sanjuan, D. R.; Aquilante, F.; Lindh, R. *Comput Mol Sci.* **2012**, *2*: 585-603.

[68] Dushek, F.; Schmitt, M.; Materny, A.; Kiefer, W. *J. Raman Spectr.* **1997**, *28*, 445-453.

[69] Li, Y.-L.; Lee, C. W.; Leung, K. H.; He, G. Z.; Phillips, D. L. *Mol. Phys.* 2002, *100*, 2659-2663.

[70] Deplano, P.; Ferraro, J. R.; Mercuri, M. L.; Trogu, E. F. *Coord. Chem. Rev.* **1999**, *188*, 71-95.

[71] Cavallo, C.; Metrangolo,P.; Milani, R.; Pilati, T.; Priimagi, A.; Resnati, G.; Terraneo, G. *Chem. Rev.* **2016**, *116*, 2478-2601.

[72] Liu, Ya-J.; de Vico, L.; Lindh, R.; Fang, W.-H. *ChemPhysChem.* **2007**, *8*, 890-898.

[73] Xiao, H.-Y.; Liu, Y.-J.; Yu, J.-G.; Fang, W.-H. *Chem. Phys. Lett.* **2007**, *436*, 75-79.

[74] Rozgonyi, T.; Gonzáles, L. *J. Phys. Chem.* **2006**, *110*, 10251-10259.

[75] Rozgonyi, T.; Gonzáles, L. *J. Phys. Chem.* **2002**, *106*, 11150-11161.

[76] Liu, K.; Zhao, H.; Wang, C.; Zhang, A.; Ma, S.; Li, Z. A *J. Chem. Phys.* **2005**, *122*, 044310.

[77] Liu, Y.-J.; Ajitha, D.; Wisborg-Krogh, J.; Tarnovsky, A. N.; Lindh, R. *ChemPhysChem* **2006**, *7*, 955-963.

[78] Kirmse, W. *Eur. J. Org. Chem.* **2005**, *2005*, 237-260.

[79] Bourissou, D.; Guerret, O.; Gabbai, F. P.; Bertrand, G. Stable Carbenes *Chem. Rev.* **2000**, *100*, 39-91.

[80] Glendening, E. D.; Weinhold, F. *J. Comp. Chem.* **1998**, *19*, 593-609.

[81] Glendening, E. D.; Weinhold, F. *J. Comp. Chem.* **1998**, *19*, 610-627.

[82] Glendening, E. D.; Badenhoop, J. K.; Weinhold, F. *J. Comp. Chem.* **1998**, *19*, 628-646.

[83] Weinhold, F.; Landis, C. R. In *Discovering Chemistry with Natural Bond Orbitals*; John Wiley & Sons, Inc., **2012**; p. 252-296.

[84] Gdanitz, R. J.; Ahlrichs, R. *Chem. Phys. Lett*. **1988**, *143*, 413-420.

[85] Xu, D.; Francisco, J. S.; Huang, J.; Jackson, W. M. *J. Chem. Phys.* **2002**, *117*, 2578-2585.

[86] Huang, H.-Y.; Chung, W.-T.; Sharma, R. C.; Hsu, C.-Y.; Lin, K.-C.; Hu, C.-H. *J. Chem. Phys.* **2004**, *121*, 5253-5260.

[87] Tu, C. P.; Cheng, H. I. Chang, B. C. *J. Phys. Chem. A*. **2013**, *117*, 13572-13577.

[88] Kovalenko, S. A.; Dobryakov, A. L.; Ruthmann, J.; Ernsting, N. P. *Phys. Rev. A* **1999**, *59*, 2369-2384.

[89] Aquilante, F.; De Vico, L.; Ferre, N.; Ghigo, G; Malmqvist, P. A.; Neogrády, P.; Pedersen, T. B.; Pitonák, M.; Reiher, M.; Roos, B. O.; Serrano-Andrés, L.; Urban, M.; Veryazov, V.; Lindh, R. *J. Comp*. *Chem*. **2010***, 31*, 224-247.

[90] Serrano-Andrés, L., Merchán M. & Lindh, R. *J. Chem. Phys.* **2005**, 122, 104107.

[91] Neese, F. *Wiley Interdiscip. Rev.: Comput. Mol. Sci.*, **2012**, *2*, 73–78.

[92] Glendening, E. D.; Landis, C. R.; Weinhold, F. NBO 6.0: *J. Comput. Chem*. **2013**, *34*, 1429-1437.

Supporting information

CH$_2$I$_2$ and CHBr$_3$: A Brief Spectroscopic Summary

The UV absorption spectrum of CHBr$_3$ is dominated by the $\widetilde{X}\,^1A_1 \rightarrow \widetilde{B}\,^1E$ transition at ~220 nm, whereas the lowest-energy singlet-singlet $\widetilde{X}\,^1A_1 \rightarrow \tilde{A}^1A_2$ transition is at 243 nm,[1] Figure 2S. Previous works suggested a unity quantum yield for the Br-atom dissociation channel upon 248 nm excitation.[2] This is in disagreement with several other studies suggesting photoelimination of both molecular and atomic bromine,[3-6] where most of the Br atoms are produced in the ground $^2P_{3/2}$ state.[3,7]
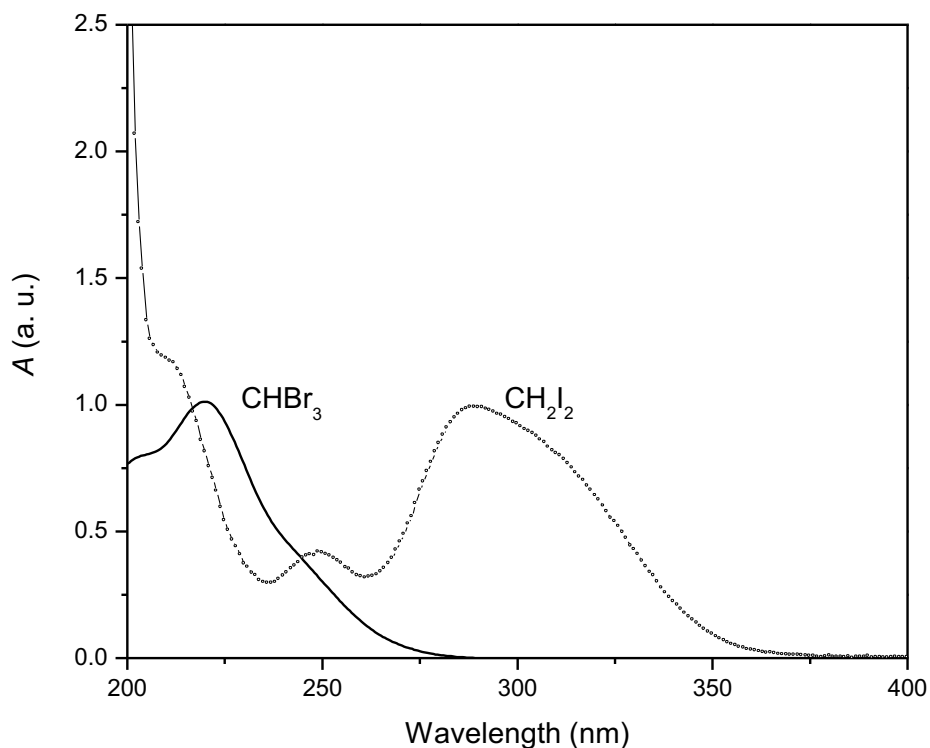

Figure S3.1. Steady-state absorption spectra of CHBr$_3$ and CH$_2$I$_2$ vapor.

For CH$_2$I$_2$ at 330 nm, only the lowest singlet excited state is reached via the $1^1A_1 \rightarrow 1^1B_1$ transition, [8-11] Figure 2. CH$_2$I$_2$ in the 1^1B_1 state dissociates exclusively yielding CH$_2$I radicals and

$I(^2P_{3/2})$ iodine atoms.[11-17] Previous photofragment spectroscopy works showed that the dissociation occurs on a time scale faster than the CH_2I_2 rotational period.[8] The low-lying excited states of CH_2I_2 computed along a single coordinate (the C−I bond length) are repulsive,[17] supporting the commonly adopted premise that the only primary photochemical event leads to the formation of the CH_2I and I fragments.

Computational Background

The description of excited electronic states generally requires a treatment of both static and dynamical electron correlation. The dynamic correlation is the result of instantaneous electron-electron repulsion. The static correlation is caused by state mixing, which is a typical situation where electronic states are near degenerate, and in consequence, in none of the states involved the wavefunction can be described by a single Slater determinant. Popular methods such as Hartree-Fock, Møller-Plesset second-order perturbation theory (MP2), or Density Functional Theory (DFT) are single-configurational, meaning that they utilize a single Slater determinant for describing the wavefunction. This approximation is valid when electronic states do not come into close energetic proximity. For the description of the photoisomerization in $CHBr_3$ because of the presence of the S_1/S_0 surface crossing along the reaction path,[18] and in CH_2I_2, where the photoisomerization is similarly rapid and the presence of a conical intersection is suspected, this approximation cannot be expected to be valid. Furthermore, the isomer minimum is situated not far from radical dissociation asymptote. There are several computational methods accounting both for static and dynamic electron correlation. Among those, the method of choice is the complete active space second order perturbation theory (CASPT2), which is accurate, and at the same time, not prohibitively expensive. CASPT2 uses a linear combination of Slater determinants as a zero-order wavefunction (and therefore, it belongs to multireference

methods[19]) and then performs energy and wavefunction corrections using perturbation theory. CAPST2 has the electronic energy accuracy < 6.9 kcal/mol in "almost all cases",[20,21] making it "a true *gold standard*" for excited-state computational studies. CASPT2, however, uses molecular orbital but not valence bond formalism. Yet, it is the latter that is useful for the description of fractional bonds and fractional charges developing in the course of a typical photochemical reaction. Despite the recent resurgence of the valence bond theory, we are not aware of any computational method that would use this language and yield correct energetics and structures for the molecules of interest. For computing resonance structures contributing to a given molecular geometry and their weights, Natural Resonance Theory (NRT) is the best algorithm known to date. NRT provides pictorially institutive structures showing bonding patterns and valence electrons that are not used in bonding. However, NRT is not compatible with CASPT2. A possible solution is single-point energy computation along the CASPT2 MEP using a method (i) compatible with NRT, (ii) with accuracy not lower than that of CASPT2. Advanced correlation methods, such as EOM-CCSD[22] or CISD,[23-25] are single reference, and as a result, they fail in the proximity of CI.[26] Thus, we have chosen the multireference averaged coupled pair functional (MRACPF), which is an improvement of MRCI (multireference configuration interaction).[27] MRACPF gives the energetics and wavefunction very similar to those of CASPT2, but is much more computationally expensive, and therefore, the use of MRACPF is unreasonable for MEP, but reasonable for single-point computations.

Figure S3.2. The active space molecular orbitals of CHBr$_3$ used for the CASPT2 calculations.
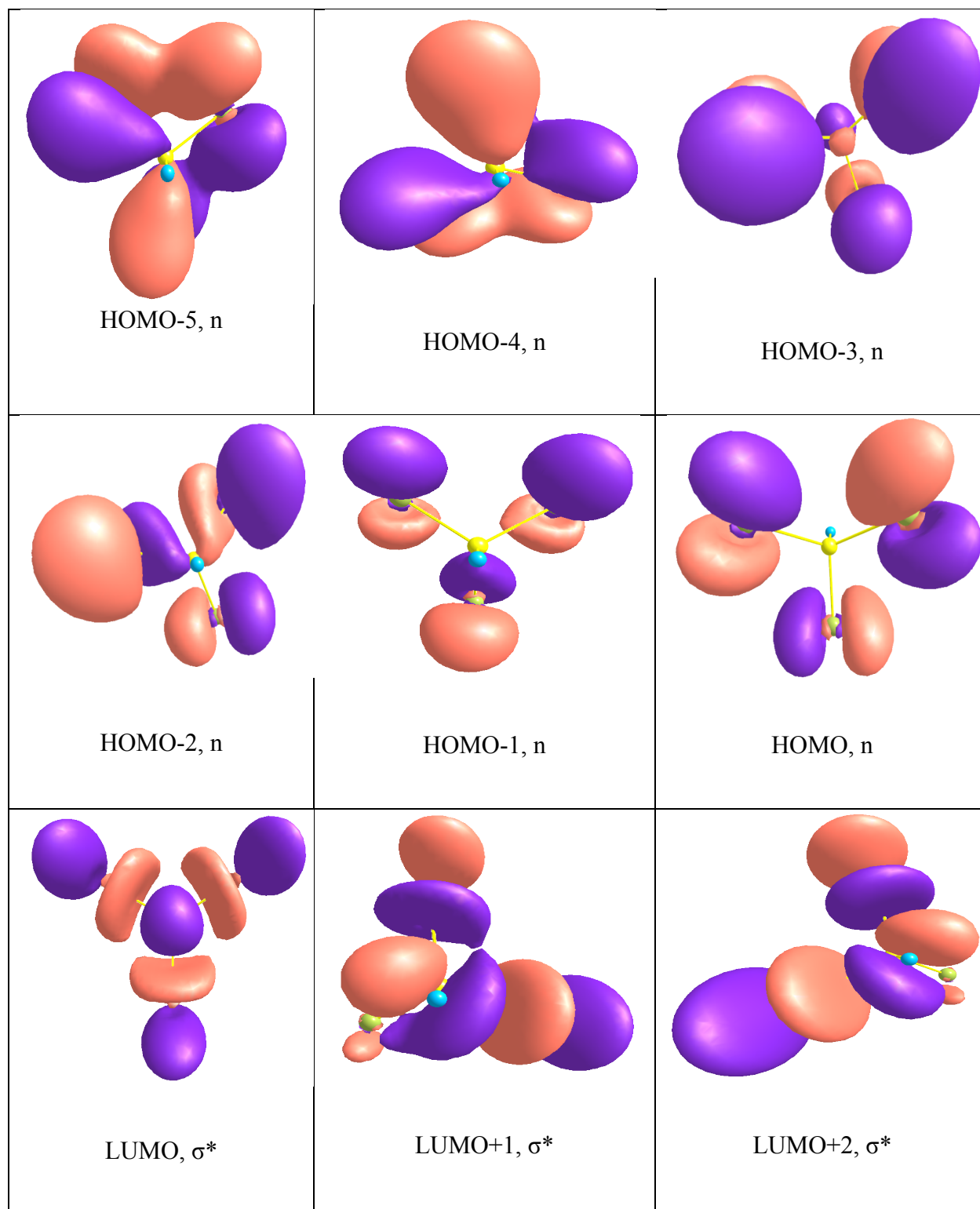

HOMO-5, n	HOMO-4, n	HOMO-3, n
HOMO-2, n	HOMO-1, n	HOMO, n
LUMO, σ*	LUMO+1, σ*	LUMO+2, σ*

Figure S3.3. The active space molecular orbitals of CH_2I_2 used for the CASPT2 calculations.
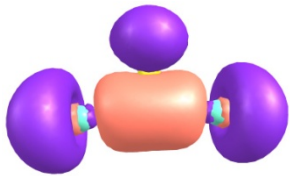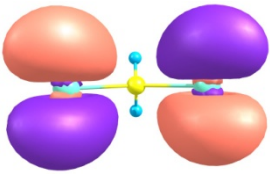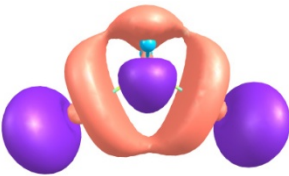
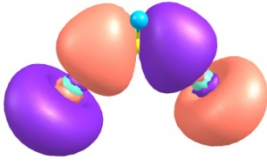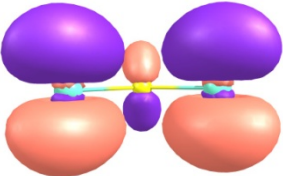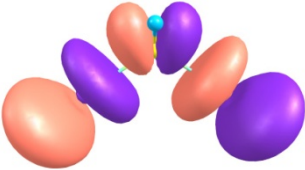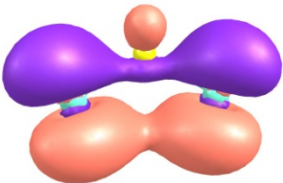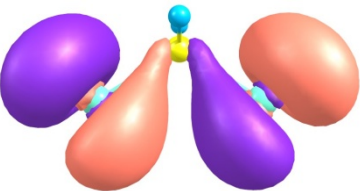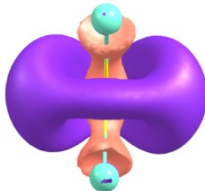|		
HOMO-5, n	HOMO-2, n	LUMO, σ*
HOMO-4, σ	HOMO-1, n	LUMO+1, σ*
HOMO-3, n	HOMO, n	LUMO+2, σ*

Table S3.1. The CASPT2 optimized structures of CHBr$_3$ and *iso*-CHBr$_3$. The interatomic distances are shown in Å, the bond angles are shown in degrees. The migrating bromine is labelled as Br(2) and the bromine-bromine bond in *iso*-CHBr$_3$ is labelled as Br(2)–Br(3).

	C–H	C–Br(1)	C–Br(3)	C–Br(2)	Br(2)–Br(3)	H–C–Br(1)	Br(1)–C–Br(3)	C–Br(3)–Br(2)	H–C–Br(3)–Br(2)
CHBr$_3$	1.08	1.94	1.94	1.94	3.22	107.0	112.0	34.2	116.5
iso-CHBr$_3$	1.08	1.86	1.81	3.99	2.74	115.8	121.9	121.5	72.8

Table S3.2. The CASPT2 optimized structures of CH$_2$I$_2$ and *iso*-CH$_2$I$_2$. The interatomic distances are shown in Å, the bond angles are shown in degrees.

	C–H	C–I(1)	C–I(2)	I(1)–I(2)	H–C–I(1)	C–I(1)–I(2)	H–C–I(1)–I(2)
CH$_2$I$_2$	1.08	2.16	2.16	3.66	107.4	32.2	119.8
iso-CH$_2$I$_2$	1.08	1.99	4.42	3.08	117.6	119.8	78.1

Table S3.3. The structural parameters along the CASPT2 MEP of CHBr₃. The first and eighth MEP points correspond to the optimized structure of CHBr₃ and the structure of *iso*-CHBr₃. The interatomic distances are shown in Å, the bond angles are shown in degrees. The migrating bromine is labelled as Br(2) and the bromine-bromine bond in *iso*-CHBr₃ is labelled as Br(2)–Br(3).

MEP point	C–H	C–Br(1)	C–Br(3)	C–Br(2)	Br(2)–Br(3)	H–C–Br(1)	Br(1)–C–Br(3)	C–Br(3)–Br(2)	H–C–Br(3)–Br(2)
1	1.08	1.94	1.94	1.94	3.220	107.0	112.0	34.2	116.5
2	1.07	1.86	1.86	2.97	3.52	115.8	120.9	57.4	120.8
3	1.08	1.87	1.87	3.57	3.94	116.2	120.1	64.7	117.5
4	1.08	1.87	1.87	3.80	4.24	116.2	120.1	63.4	111.7
5	1.08	1.86	1.87	3.75	4.08	116.9	120.3	66.6	125.7
6	1.08	1.86	1.81	3.76	2.94	116.6	119.6	101.7	103
7	1.08	1.87	1.80	3.92	2.71	115.9	121.2	119.2	102.7
8	1.08	1.87	1.81	4.15	2.72	115.2	123.6	131.2	113.4

Table S3.4. The structural parameters along the CASPT2 MEP of CH_2I_2. The first and eighth MEP points correspond to the optimized structure of CH_2I_2 and the structure of *iso*-CH_2I_2. The interatomic distances are shown in Å, the bond angles are shown in degrees.

MEP step	C–H	C–I(1)	C–I(2)	I(1)–I(2)	H–C–I(1)	C–I(1)–I(2)	H–C–I(1)–I(2)
1	1.08	2.16	2.16	3.66	107.4	32.2	119.8
2	1.08	2.07	3.06	3.89	115.6	51.5	72.9
3	1.08	2.07	3.52	4.15	116.5	57.9	77.1
4	1.08	2.06	3.94	4.20	117.3	68.5	80.8
5	1.08	2.06	4.20	4.20	117.3	75.5	80.8
6	1.08	2.04	4.15	3.72	116.9	86.9	79.7
7	1.08	2.00	4.10	3.26	117.2	99.7	78.7
8	1.08	1.99	4.34	3.08	117.4	116.1	78.2
9	1.08	2.01	4.68	3.10	118.0	131.0	78.6

Table S3.5. Some of interesting resonance structures (X = Br or I), including those previously considered for the *iso*-CH$_2$I$_2$ and *iso*-CHBr$_3$ species by Maier, Reid and co-workers, which contribution in this work is found to insignificant along the entire MEP (<5%).

| Resonance structures	*iso*-CHBr$_3$	*iso*-CH$_2$I$_2$
Three-body dissociation species		
Radical species produced via H-atom dissociation		
Carbene-dihalogen complex		
Three-center four-electron hypervalent		
Open-shell singlet born out from a halide-halocarbenium contact ion pair by decoupling the C-X double bond		
Contact ion pair with a positively charge on the carbon atom and a negative charge on the outer X atom		
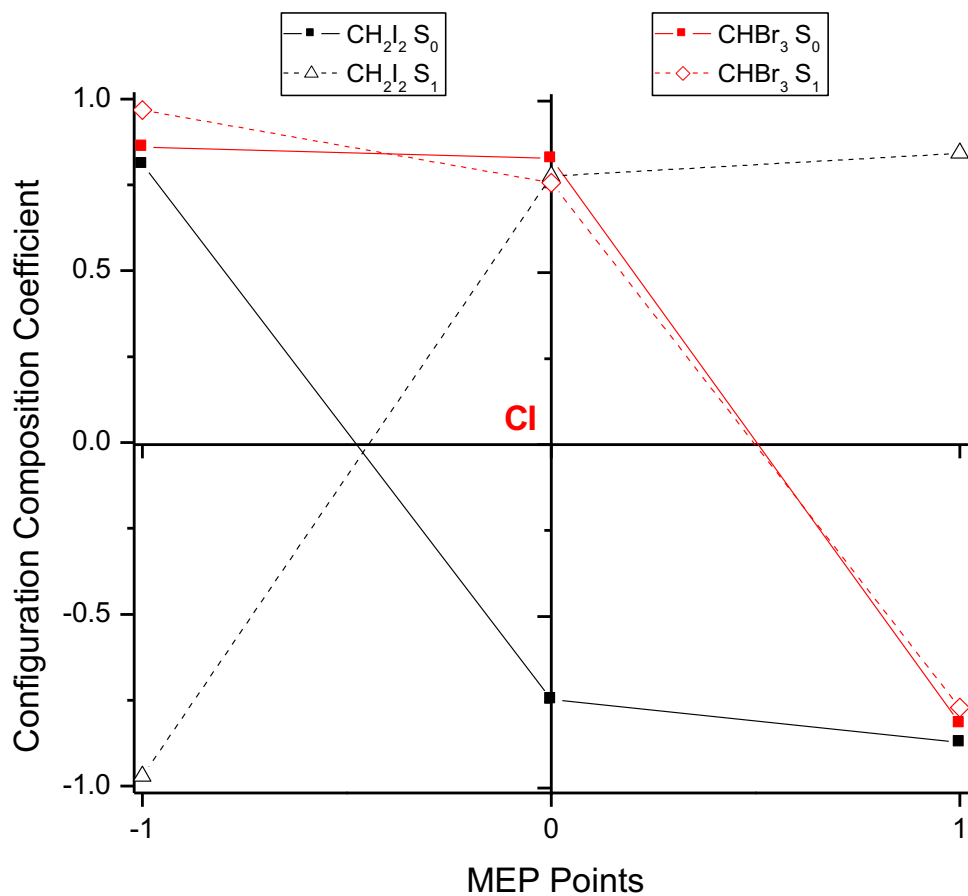
Figure S3.4. Configuration composition coefficients of the major configuration contributing to the composition of the S_0 and S_1 wavefunction of $CHBr_3$ and CH_2I_2 illustrate the geometrical phase effect.[28] Upon going along the MEP from the point preceding the conical intersection (labelled as CI) to the next point after the CI, the coefficients reverse their sign, indicating the change of the sign of the wavefunction.

References

[1] Mereshchenko, A. S.; Butaeva, E. V.; Borin, V. A.; Eyzips, A. E.; Tarnovsky A. N. *Nature Chem*. **2015**, *7*, 562-568.

[2] Peterson, K. A. Francisco, J. S. *J. Chem. Phys*. **2002**, *117*, 6103-6107.

[3] Zou, P. Shu, J. Sears, T. J. Hall, G. E. North, S. W. *J. Phys. Chem. A* **2004**, *108* 1482-1488.

[4] Xu, D.; Francisco, J. S.; Huang, J.; Jackson, W. M. *J. Chem. Phys*. **2002**, *117*, 2578-2585.

[5] Huang, H.-Y.; Chung, W.-T.; Sharma, R. C.; Hsu, C.-Y.; Lin, K.-C.; Hu, C.-H. *J. Chem. Phys*. **2004**, *121*, 5253-5260.

[6] Bayes, K. D.; Toohey, D.W.; Friedl, R. R.; Sander, S. P. *J. Geophys. Res*. **2003**, *108*, 4095, doi:10.1029/2002JD002877, D3.

[7] Lin, K.-C.; Tsai, P.-Y. *Phys. Chem. Chem. Phys*. **2014**, *16*, 7184-7198.

[8] Tang, Y.; Ji, L.; Tang, B.; Zhu, R.; Zhang, S.; Zhang, B. *Chem. Phys. Lett*. **2004**, *392*, 493-497.

[9] Kawasaki, M.; Lee, S. J.; Bersohn, R. *J. Chem. Phys*. **1975**, *65*, 809-814.

[10] Gedanken, A.; Rowe, M. D. *Chem. Phys*. **1979**, *36*, 181-186.

[11] Zhang, J.; Imre, D. G. *J. Chem. Phys*. **1988**, *89*, 309-313.

[12] Ito, M.; Huang, P.-K.; Kosower, E. M. *Trans. Faraday Soc*. **1961**, *57*, 1662-1673.

[13] Baughcum, S. L.; Leone, S. R. *J. Chem. Phys*. **1980**, *72*, 6531-6545.

[14] Koffend, J. B.; Leone, S. R. *Chem. Phys. Lett*. **1981**, *81*, 136-141.

[15] Hunter, T. F.; Kristjansson, K. S. *Chem. Phys. Lett*. **1982**, *90*, 35-40.

[16] Jung, K.-W.; Ahmadi, T. S. El-Sayed, M. A. *Bull. Korean Chem. Soc*. **1997**, *18*, 1274-1280

[17] Xu, H.; Guo, Y.; Liu, S.; Ma, X.; Dai, D.; Sha, G. *J. Chem. Phys*. **2002**, *117*, 5722-5729.

[18] Liu, Ya-J.; de Vico, L.; Lindh, R.; Fang, W.-H. *ChemPhysChem*. **2007**, *8*, 890-898.

[19] Mereshchenko, A. S.; Butaeva, E. V.; Borin, V. A.; Eyzips, A.; Tarnovsky, A. N. *Nature Chem*. **2015**, *7*, 562-568.

[20] The description of configuration interaction is based on the expansion of the wavefunction in a set of Slater determinants each of which corresponds to a specific excitation of the ground state electronic configuration. The Slater determinant from which the excitations are performed is called reference function. If the excitations are performed from a single Slater determinant, the methods are called single-reference. If the excitations are performed from a linear combination of a number of Slater determinants, the corresponding methods are called multireference.

[21] Pulay, P. A. *Int. J. Quant. Chem.* **2011**, *111*, 3273-3279.

[22] Sanjuan, D. R.; Aquilante, F.; Lindh, R. *Comp. Mol. Sci.* **2012**, *2*: 585-603.

[23] Koch, H. & Jørgensen, P. *J. Chem. Phys.* **1990**, *93*, 3333-3344.

[24] Pople, J. A.; Seeger, R.; Krishnan, R. *Int. J. Quantum Chem*. **1977**, *12*, 149-63.

[25] Raghavachari, K.; Schlegel, H. B.; Pople, J. A. *J. Chem. Phys.***1980**, *72*, 4654-4655.

[26] Raghavachari K.; Pople, J. A. *Int. J. Quantum Chem.* **1981**, *20*, 1067-1071.

[27] Li, X.; Paldus, J. *Adv.Chem.Phys.* **1999**, *110*, 2844-2852

[28] Gdanitz, R. J.; Ahlrichs, R. *Chem. Phys. Lett*. **1988**, *143*, 413-420.

[29] Longuet-Higgins H. C. *Proc. R. Soc. London Ser. A* **1975**, *344*, 147-156.